GEM TN-92-150

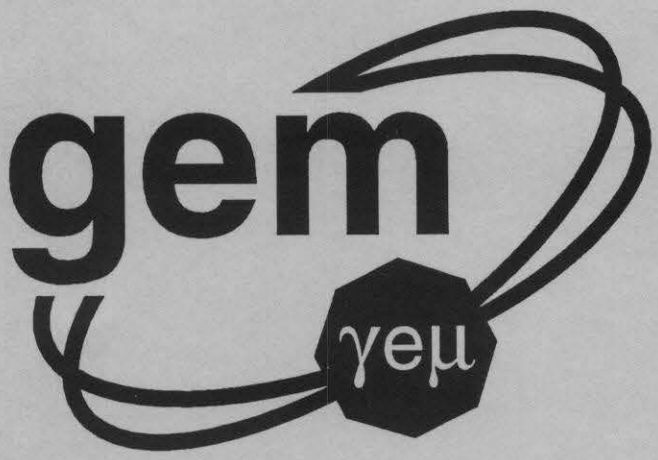

Analysis of an Alignment Scheme for the GEM Muon Barrel

J. Paradiso
C.S. Draper Laboratory

October 1992

Abstract:

An analysis package has been developed to investigate an alignment scheme defined for the GEM muon barrel. Individual chambers can be arbitrarily translated and/or rotated, and sagitta corrections are calculated from a system of alignment monitors. The sagitta error, correction, and residual are plotted (vs. θ and ϕ) for straight-line tracks arising from the IP. Using this package, intuition may be developed into the accuracy and nature of particular alignment corrections. Several effects have been found to limit the error correction to the percent or permil levels for certain chamber deflections, which may become significant for large misalignments.

Analysis of an Alignment Scheme for the GEM Muon Barrel

-- J. Paradiso, Oct. '92

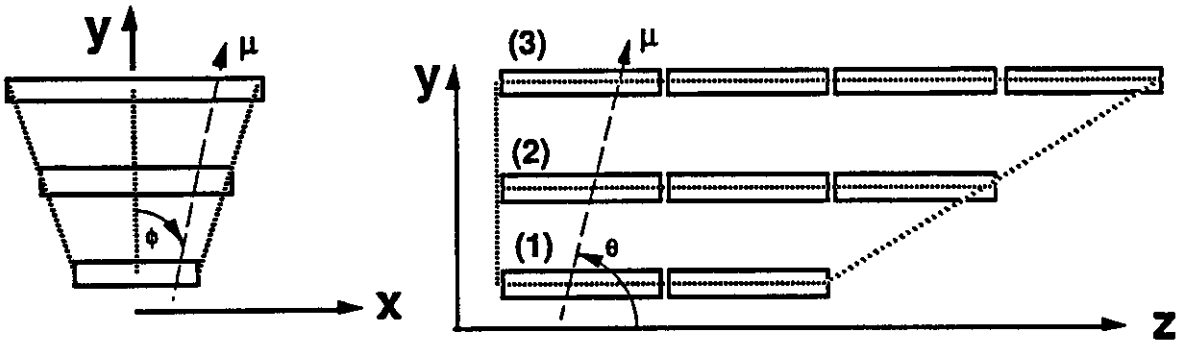

Figure 1: Schematic of the muon alignment scheme adopted in the simulations

1) Motivation, Strategy, and Analysis

The alignment requirements[1,2] needed to attain the required momentum precision in the GEM muon barrel are extremely demanding. The most exacting of these specifications are driven by the 25 μm alignment error allowed in the bending coordinate (here referred to as "x"). In order to attain such accuracy, it has been proposed[3] to dynamically measure the deviation of the chamber systems from perfect alignment using precision alignment monitors such as LED/LENS[4] or RASNIK[5] systems (for layer-to-layer alignment) and multi-point monitors such as stretched wires[6,7] or nested 3-point optical monitors[8] to determine inter-chamber alignment within a layer. A rough diagram of such a system applied to the GEM muon barrel is depicted in Fig. 1. The multipoint monitors (which measure the displacements of the chamber corners from the line between the layer endpoints) run horizontally along z on each side of a superlayer. Six projective 3-point LED-LENS straightness monitors run between superlayers (a pair on each side with monitors connecting the four superlayer corners, plus a pair in the center). The horizontal multipoint monitors measure the corrections needed to effectively "straighten" a superlayer, while the projective 3-point monitors measure the displacement of the three layers in the bending coordinate. The simple scheme depicted in Fig. 1 is somewhat idealistic, in that it provides the minimal set of measurements needed to correct misalignments. The accuracy of an actual deployed system would benefit considerably from additional projective monitors and multipoint sensors, as will be discussed in the conclusion of this report.

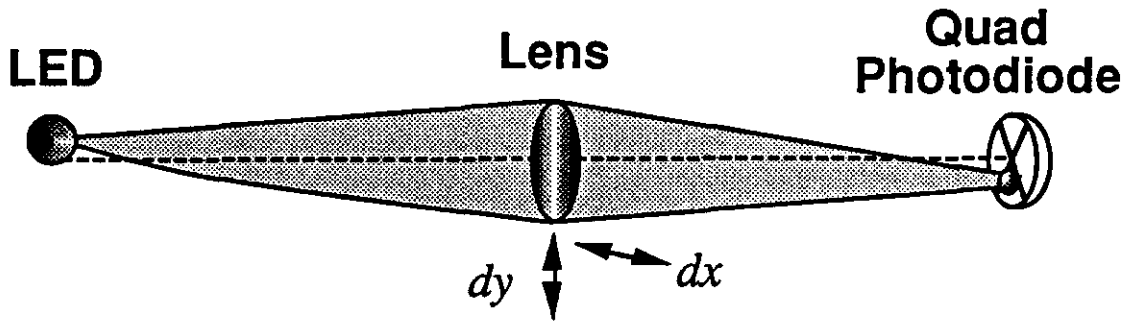

Figure 2: The standard 3-point optical straightness monitor

In order to access the performance of alignment schemes such as suggested in Fig. 1, several simulations have been (or are being) written to determine alignment corrections from postulated monitor systems and evaluate their accuracy. One of these routines[9] randomly perturbs (i.e. rotates, translates) chamber superlayers about all axes, and statistically evaluates the alignment correction for arbitrary chamber motions; such a verification is essential in guaranteeing the performance of any alignment layout. The software developed under this study takes a different tack, however, in that a specific chamber misalignment is generated (the chambers and layers may be translated, rotated, or scaled as desired), and the alignment correction and residual (for straight-line tracks) are then plotted across the entire superlayer θ,ϕ span for visual analysis.

Because the local alignment requirements are so exacting, small, higher-order effects can become quite significant, especially with large displacement errors (i.e. it has been suggested[3] that the GEM alignment monitors be designed to yield a dynamic range approaching ±5 mm, within which an alignment correction could be made in the muon reconstruction software). This study has investigated several such effects, and simulation results are presented in this report. Together with the analysis technique of Ref. [9], these error sources can be identified, understood, and their effect on the muon momentum reconstruction appropriately limited.

The standard 3-point optical straightness monitor is shown in Fig. 2. It measures the displacement of the optical center of a lens from the line between the light source (conventually a smooth-aperture LED with a square collimator) and a receiver (generally a quadrant photodiode; potentially a lateral-effect photodiode or CCD array). The ideal measurement may be easily parameterized in vector notation:

1) $$\vec{\Delta}_a = (\vec{r}_{12} \times \vec{r}_{13}) \times \vec{r}_{13}$$

$\vec{r}_{13}$ = Vector from source to receiver
$\vec{r}_{12}$ = Vector from source to lens

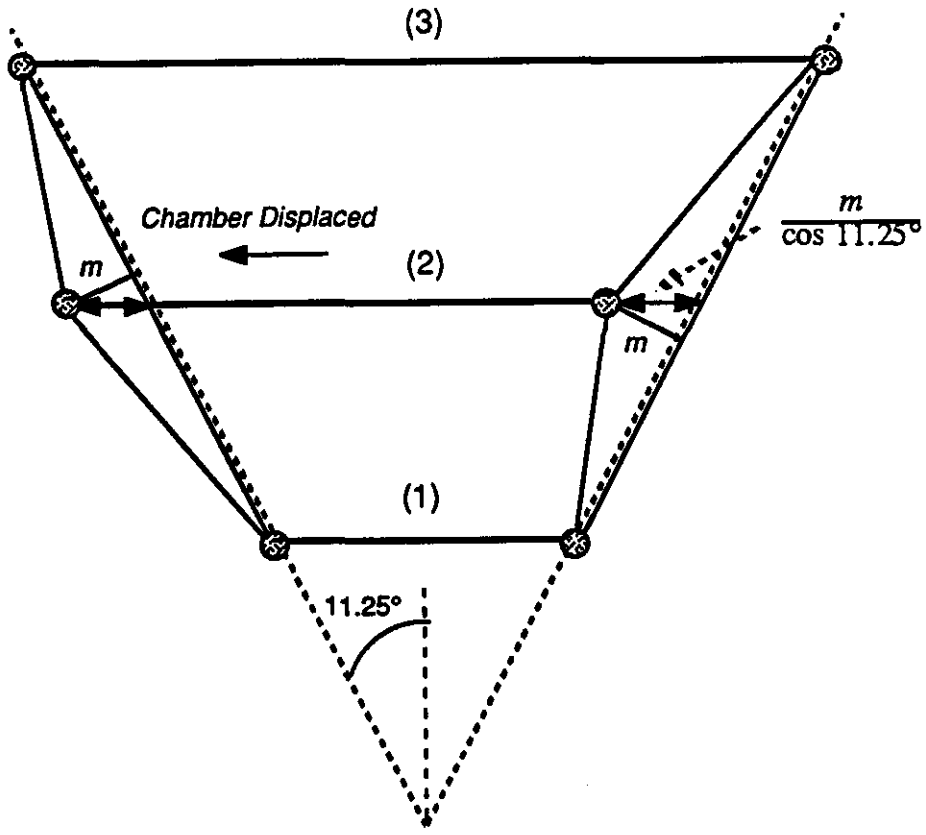

Figure 3: Straightness Monitor measurement of middle superlayer displacement

The straightness monitors of Fig. 2 have an implicit gain of 2 in their measurement, which is not included in Eq. 1. In addition, there are several other effects that can enter, which are unaccounted for here. If the lens is translated along the line between source and receiver, a change in magnification will result, effectively displacing the measurement. In addition, the receiver essentially performs a centrioding operation over the projected image of the source; due to nonlinearity inherent in the receiver response to displacement, the measured position can change with the size of the source image, which is also a function of the spacing of the 3 elements along the source-detector line. Granted, such effects are generally small, but should be included in future simulations; as is shown in this study, combinations of minor errors can become significant when large alignment corrections are required.

The vector $\vec{\Delta}_z$ has essentially 2 components perpendicular to $\vec{r}_{13}$. The relevant component of this measurement (m) is also perpendicular to the magnetic field direction (which is assumed to always point along the z-axis). The component orthogonal to this

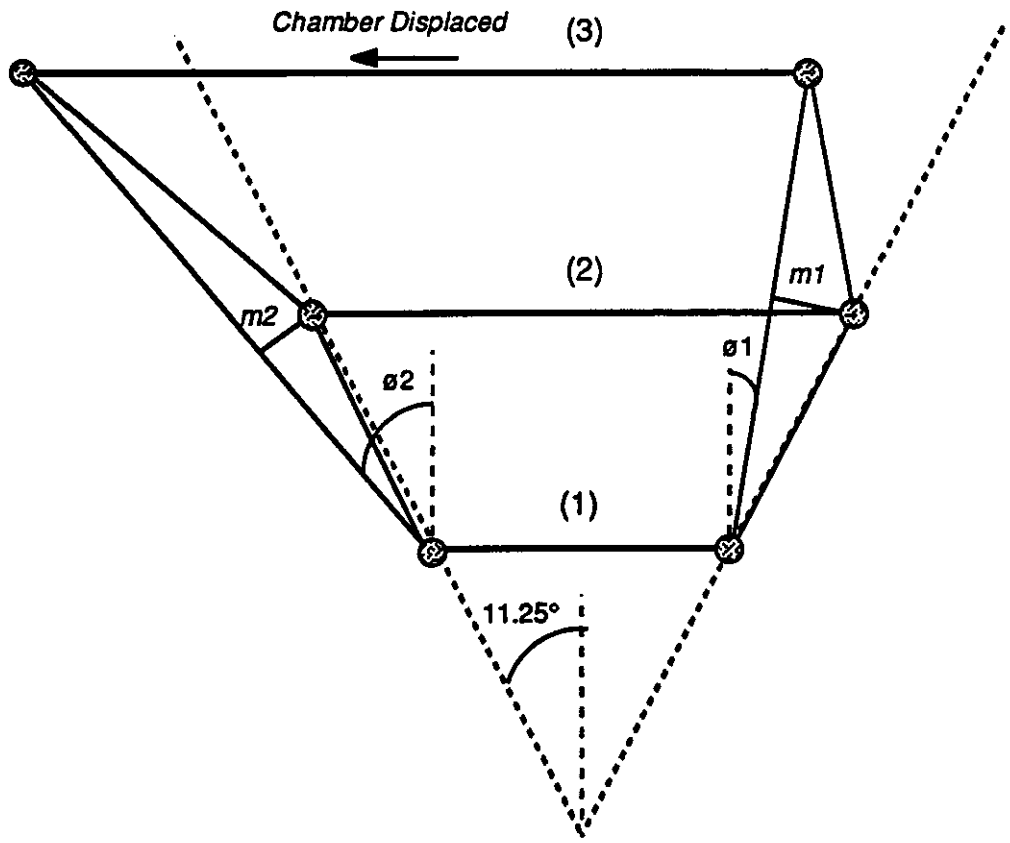

Figure 4: Straightness Monitor measurement of top superlayer displacement

(q) is not directly related to the sagitta error (although still may be of beneficial use in an estimator, which will be discussed later). These components can thus be described:

2)
$$m = \vec{\Delta}_a \cdot (\vec{z} \times \vec{r}_{13})$$
$$q = \vec{\Delta}_a \cdot ([\vec{r}_{13} \times \vec{z}] \times \vec{r}_{13})$$

The straightness monitors thus measure the normal distance between the lens and the line connecting the source and receiver. The chambers, however, ideally measure the intercept of a track along a plane. If they are displaced, the sagitta errors in the reconstructed muon momenta appear along the plane of the chamber, not along the normal to $\vec{r}_{13}$ that is directly measured by the monitors. The situation is depicted in Fig. 3, which shows a middle chamber displaced excessively along the sagitta axis. In order to derive the appropriate quantity, the monitor measurement m must be divided by the cosine of the angle between the straightness monitor axis $\vec{r}_{13}$ and the normal to the chamber planes (here assumed to be 11.25°, which is the half-angle in ϕ subtended by the GEM hexants).

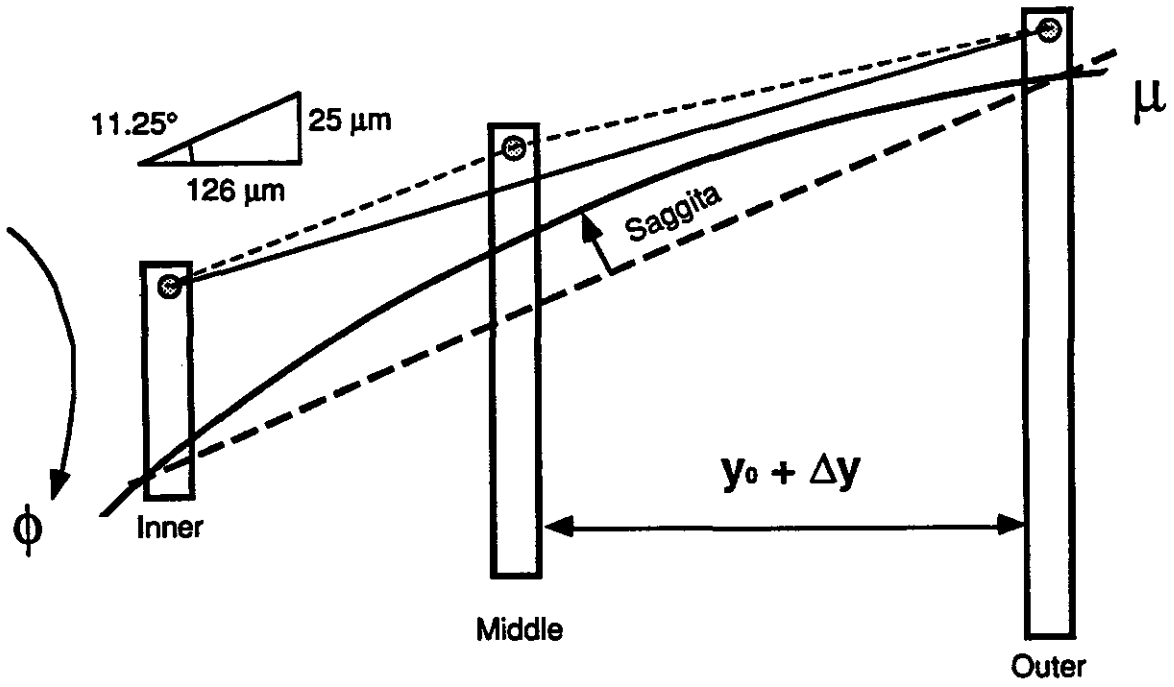

Figure 5: Sagitta error from radial shift of middle chamber position

This effect can introduce limited errors; i.e. since the angle between $\vec{r}_{13}$ and the chamber plane normal is not measured, it must be assumed at a default value (i.e. 11.25°, as in Fig. 3). As the chambers shift, however, this assumption looses validity. Fig. 4 shows a simple example of this effect; i.e. the top chamber is shifted (here by an exaggerated amount) in the sagitta direction. As a result, the sagittas measured at each side of the hexant are different [$m1 > m2$] (although this effect will not be seen by the straight-line muon coordinates in the chamber intercepts), and because the angles between the straightness monitor axes and middle chamber plane are assumed to still be identical (certainly untrue here; $\phi 1 \neq \phi 2$), different sagitta corrections will be applied at each hexant edge. This causes a non-zero second order correction (as described below) to be applied to the muon sagitta vs ϕ, which produces an error; the actual correction should be uniform.

Another chamber displacement that can induce a sagitta error is a radial motion of the chamber planes; i.e. a change in distance between layers 1 & 2 or 2 & 3. This causes the edges of the hexants to become non-projective, as illustrated in Fig. 5. In Ref. [1], the error from this source was parameterized by $\Delta x = \Delta y \tan\phi$, where Δx is the sagitta error, and Δy is the radial offset from the ideal chamber position (this is noted in the triangle drawn at upper left of Fig. 5, where we see that a radial shift of the middle chamber by 126 μm will expend the net alignment error budget of 25 μm at the hexant edges).

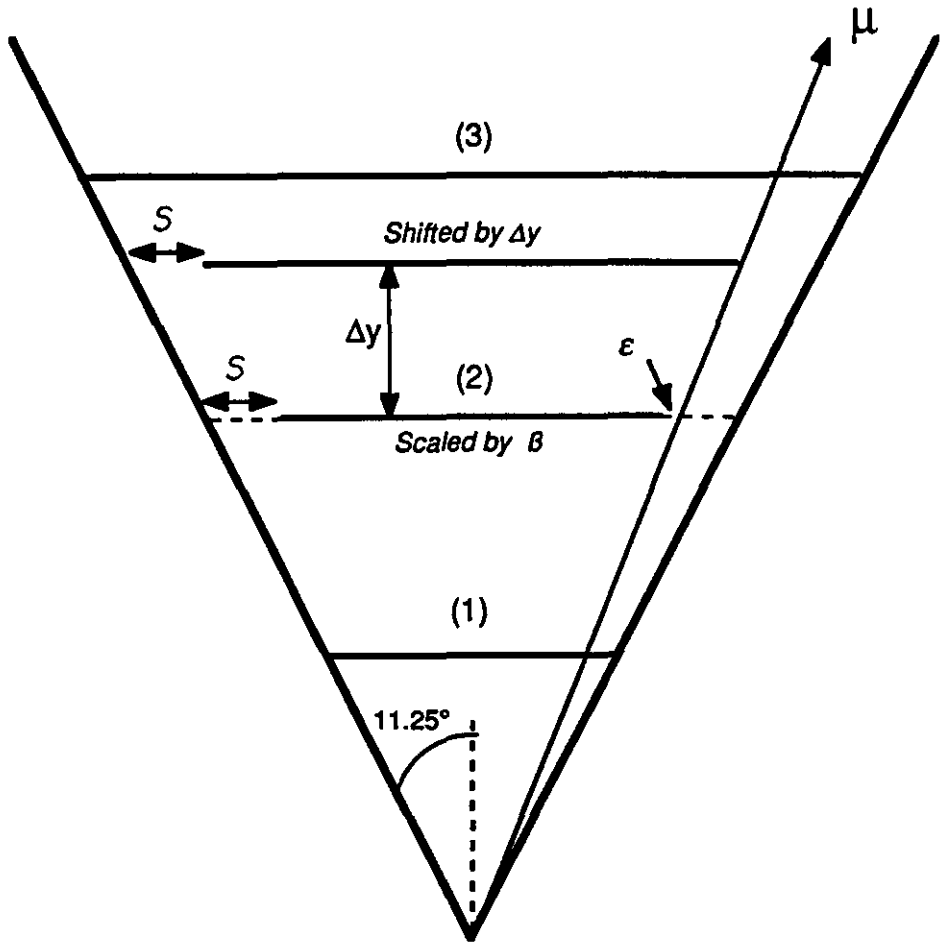

Figure 6: Comparison of errors due to radial shift and longitudinal scaling of middle superlayer

This correction, however, is not exact. A radial shift of a chamber layer (i.e. the middle layer as shown in Figs. 5 & 6), also changes the relative ϕ intercepts between the three layers. If one goes through a sagitta calculation of the standard form:

3) $$\Delta x = (x_2 - x_1) - (x_3 - x_1)\,(y_2 - y_1)/(y_3 - y_1)$$

where the "y" coordinates are the locations of the chamber planes from the IP (folding in the Δy errors of Figs. 5 & 6), one derives the relation (for a displacement of the middle layer by Δy):

4) $$\Delta x = \left(\frac{y_2}{y_2 + \Delta y}\right) \Delta y \tan\phi$$

The alignment monitors, however will measure a slightly different result; they read as $s = \Delta y \tan\phi$ (after dividing the raw measurement by the directional cosine, as illustrated in Fig. 3). By incorporating the sagitta measurement into the assumed position of the straightness monitors (i.e. adding the Δx measured by the monitors into the nominal monitor ϕ locations used in fitting the sagitta correction), this error may be completely accounted for, and the projective monitors are able to totally cancel radial movement of the middle chamber (and greatly attenuate movement of the inner and outer chambers; the effect noted in Fig. 4 holds here as well!). The correction for static shifts (i.e. Figs. 3 & 4) remains unaffected under this assumption.

A difficulty arises here, however, in also accounting for scale changes. Assuming that a chamber endplate is an ideal metal slab that expands uniformly with temperature (which certainly needs verification for the required level of accuracy), thermal shifts will cause a scale change in the chamber endplates, most critically in the bending (x) direction. This is illustrated in Fig. 6, where the middle chamber has shrunk by a factor of ß. Running through the sagitta analysis of Eq. 3 yields a much simpler result; in this case, $\Delta x = s$ directly; i.e. the sagitta that is measured by the monitors is equal to that experienced by a muon traversing at the edge of the hexant. The additional factor in parenthesis in Eq. 4 does not apply here, thus if one modifies the correction fit ordinates as described above, a small error can be produced (this error can nonetheless approach tens of microns for a measured s around 5 mm, which becomes significant for the GEM muon system).

The above argument illustrates that these projective sagitta alignment measurements are inadequate for a complete error correction. Fig. 6 shows (an exaggerated) situation where a displaced middle layer (Δy) and scaled middle layer (ß) will produce the same measurement on the straightness monitors. As discussed, however, the exact sagitta correction is different in each case. This is illustrated by the projective muon line drawn at the edge of the hexant in Fig. 6. Although the alignment monitors will measure "s" in both cases, the intercepts on the displaced and scaled layer are different (the discrepancy is denoted as ε), thus their reconstructed sagittas will likewise differ.

The dilemma posed by this situation may be resolved in a variety of fashions. By using the information in the other straightness monitor coordinate (they are, afterall, 2-axis sensors), the ambiguity could potentially be broken. This is not directly possible here, however, since the monitor set at $\theta = 90°$ is unable to independently measure the y-coordinate, and the monitors at $\theta = 30°$ also couple in the z displacements. The compromise that may evict the best performance (without changing the monitor system)

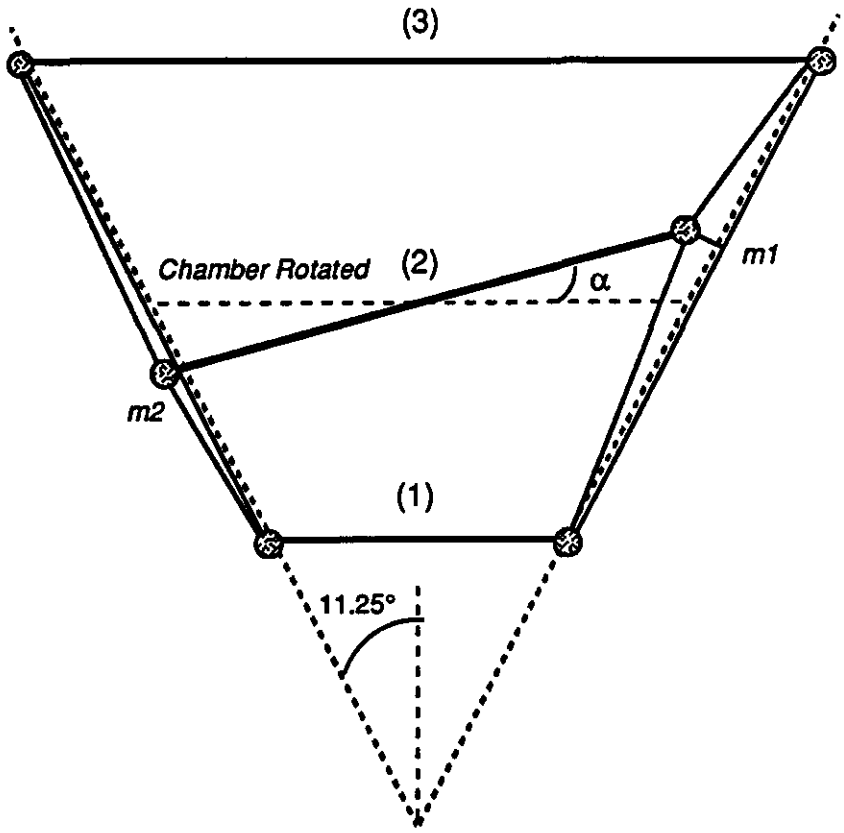

Figure 7: Rotation of Middle Superlayer about z-axis

is to not redefine the fit ordinates (as discussed above), but apply the sagitta corrections directly to completely cancel out scaling shifts (assuming that these will be significantly present; of course, this depends on the endplate composition and expected thermal environment). This will, however, enhance the error arising from radial chamber displacement, but these motions are already attenuated by a factor of tan ϕ (where the maximum ϕ is currently 11.25°), thus their contribution to the error budget will be smaller.

As noted in Ref. [10], a rotation of a chamber layer about the z (beam) axis will induce a quadratic dependance of the sagitta correction on the ϕ angle (or more specifically on tan ϕ). This can be illustrated by a simple example, where the middle chamber layer is rotated about its center by an angle α, depicted in Fig. 7. The direct sagitta error is $\Delta x_0 = y_2 \tan \phi (1 - \cos \alpha)$, where y_2 is radial superlayer position. An error also comes about from the Δy displacement; assuming the tangent approximation, we derive: $\Delta y = y_2 \tan \phi \tan \alpha$. Putting this all together, we get:

5) $$\Delta x_{net} \approx \Delta y \tan \phi + \Delta x_0 = y_2 [\tan^2 \phi \tan \alpha + \tan \phi (1 - \cos \alpha)]$$

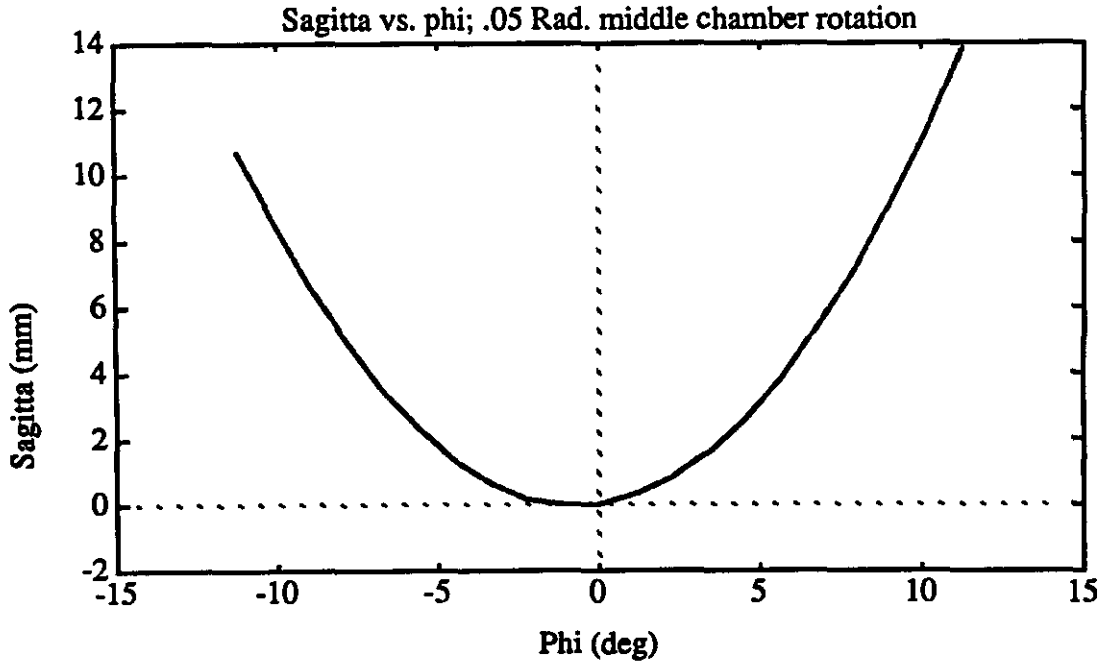

Figure 8: Calculated sagitta for z-rotation of middle superlayer

Eq. 5 is obviously quadratic in tan ϕ. It has been plotted vs. ϕ for a rotation of $\alpha = .05$ rad in Fig. 8. The differing sagitta values seen at each hexant edge can also be noted in Fig. 7 (a result of the projective geometry), and are seen in the simulated data. The sagitta error at $\phi = 0$ must remain zero (since the chamber doesn't translate here), although the $\phi = 0$ value is not at the quadratic minimum; it is generally at one of the two roots (the sagitta goes slightly negative at the minimum). Granted, this is a simple example. In reality, there will be a superposition of rotations and translations of all chamber packages. Although the coupling of rotations and translations of the various layers can induce additional projection errors, the form of Eq. 5 (with offset terms added for the translations) is seen to hold over a moderate range of possible deflections.

As seen in Fig. 7, the straightness monitors will produce sagitta measurements of the same sign, which can not be distinguished from a chamber scaling/displacement by the two edge-running monitors that are shown. This study has taken the suggestion of Ref. [10]; i.e. a third straightness monitor system is assumed to be installed at $\phi = 0$ (the baseline arrangement outlined in Ref. [3] assumed that the radial y-coordinate would be independently measured by instrumented zerodur rods, eliminating this problem, albeit at some complication). This triple measurement determines a unique quadratic, parameterized as:

6) $\Delta x = Aq^2 + Bq + C$ *Where:* $q = \tan \phi$ for muon intercept in middle chamber

$$A = \frac{\frac{(s_1 - s_3)(q_1 - q_2)}{(q_1 - q_3)} - (s_1 - s_2)}{\frac{(q_1^2 - q_3^2)(q_1 - q_2)}{(q_1 - q_3)} - (q_1^2 - q_2^2)} \qquad B = \frac{(s_1 - s_3) - A(q_1^2 - q_3^2)}{(q_1 - q_3)} \qquad C = s_1 - B\,q_1 - A\,q_1^2$$

The values s_1, s_2, s_3 are the sagittas measured by the 3 monitors located at positions q_1, q_2, q_3 (which are stated in terms of $q_i = \tan \phi_i$ the coordinates of the middle chamber have been assumed in the fits used here). The correction for monitor displacement discussed earlier has been applied in the specification of these coordinates by adding the measured sagittas into the x positions:

7) $$q_i = (x_{i(2)} + s_i)/y_2$$

where $x_{i(2)}$ is the nominal monitor position on the middle chamber plane, and y_2 is the nominal radial position of the middle plane. Granted, these corrections decrease sensitivity to rotations and Δy displacements, but will increase sensitivity to thermal scaling shifts (as discussed earlier), thus may not be advisable to employ in practice.

The rotations were seen to also be better fit if an additional correction was incorporated into the quadratic term. After a sagitta Δx was derived via Eq. 6, a new ordinate was determined in a similar fashion to Eq. 7:

8) $$q' = (y_2 \tan \phi + \tfrac{1}{2} \Delta x)/y_2$$

The sagittas are then re-calculated through a modified version of Eq. 6:

9) $$\Delta x = Aq'^2 + Bq + C$$

The effect of these corrections can be debated. Granted, they can produce significant benefit for certain layer misalignments, but can increase the error budget for others, as has been demonstrated above in the Δy vs. scaling case. More investigation is warranted...

If the chamber is rotated about the x or y axes, the sagitta error will change linearly with the z-coordinate. As a result, a linear z interpolation must be performed between the monitors located at $\theta = 90°$ and $\theta = 30°$. This can be prone to several errors. The superlayer misalignment in z resulting from the rotation will produce a shift in the measured θ (analogous to the shifts in measured ϕ that were discussed above), which can

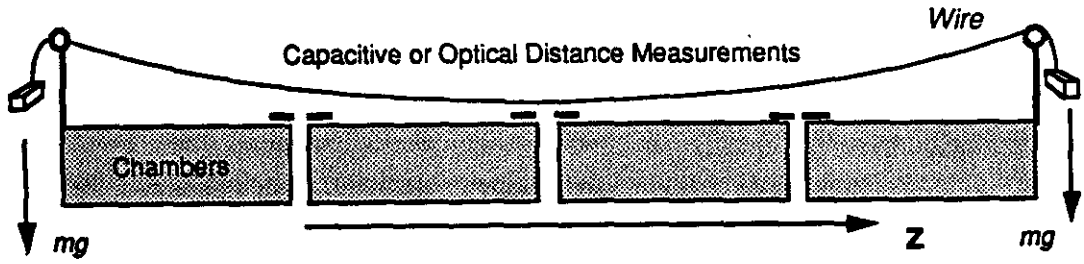

Figure 9: Application of stretched-wire technique to align chamber packages in a superlayer

generate an error in the interpolation ordinates. This can be reduced by straightening the muon tracks in the nonbending rθ plane; i.e. these lines must be straight (ignoring scattering effects and nonuniform magnetic fields), thus the middle chamber measurement can be compensated to maintain a straight line. Although this is seen to improve the sagitta correction in the simulations, it leads to another potential problem; i.e. the measurement of the z-coordinate is fairly coarse (as performed with RPC strips on the order of 3.5 cm wide on the outer chamber, yielding a σ of roughly 1 cm), thus such a precise correction may not be possible. This z resolution will also induce another error into the a z-interpolation (as needed to recover from an x or y rotation) of $0.7\%/\sqrt{3}$ across the length of a superlayer (assuming a least-squares fit across projectively-sized strips in each layer), which isn't too bad...

The x and y offsets of individual chamber packages in a superlayer are measured by a set of multipoint monitors running along the z-axis. In this fashion, the superlayer is made analytically straight; i.e. the positions of each chamber are compensated in the reconstruction analysis, such that a straight line runs between the locations of the projective 3-point monitors at $\theta = 30°$ and $\theta = 90°$. The all-projective scheme of Ref. [10] proposes running inter-superlayer projective monitors to each chamber, rather than relying on the minimal set of measurements at the 90° and 30° superlayer endpoints and multipoint sensors to "straighten" the chambers mounted in-between. Since the all-projective scheme delivers additional relevant information (i.e. the direct relation between superlayers at each chamber), it is an attractive prospect. The implementation of this strategy, however, depends on the superlayer structure; i.e. all chambers must be differently sized in each superlayer such that the endplates (or alignment references) are all projective to the IP. This can create appreciable gaps in the θ acceptance, depending on the chamber design and how closely the chambers can be packed (of course, they can always overlap, but this will potentially block the alignment lines of sight). Regardless, this alternative is attractive, provided the engineering problems are satisfactorily resolved.

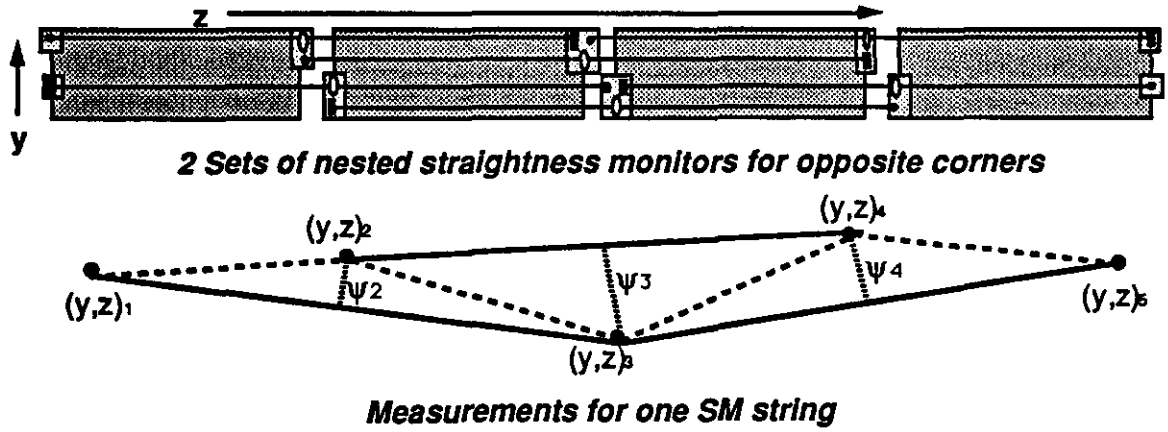

Figure 10: Application of nested straightness monitors to multipoint measurements in a superlayer

A potential solution, currently being discussed, is to run projective monitors wherever possible, to be complimented by multipoint monitors running along the z-axis. This will yield redundant information, which can be processed by an optimal estimator[11] to provide better alignment accuracy (potentially more robust to sensor noise and failure).

The alignment scheme assumed in this study adopts the sensor configuration sketched in Fig. 1. The inter-chamber multipoint measurement along z is performed in two independent fashions. One technique is the stretched wire approach[6,7], where a wire is stretched between the superlayer endpoints, and the distance from the wire to fiducials on the chamber is derived (optically or capacitatively), after correcting for the known wire sag. The analysis models this method in a very simple fashion, based on Eq. 1:

$$10) \quad \vec{\Delta}_i = (\vec{r}_{1i} \times \vec{r}_{1N}) \times \vec{r}_{1N}$$

$\vec{r}_{1N}$ = Vector from 90° edge to 30° edge
$\vec{r}_{1i}$ = Vector from 90° edge to chamber endplate #i

The application of the stretched wire approach to a 4-chamber superlayer is depicted in Fig. 9. Position sensors that reference the wire are placed at the edges of each chamber. If warping of the chambers along the z-axis is of concern (potentially a problem with cathode strip chambers), it may prove desirable to place additional position sensors along the chamber length.

The other technique used by this analysis to align chambers in a superlayer is the nested 3-point optical monitor approach, as depicted in Fig. 10. Here, standard 3-point optical monitors (as in Fig. 2) are "leapfrogged", such that they are overlapped by half of an alignment string (i.e. the first lens also has an LED for another monitor, the first

detector has a lens for the second monitor and an LED for a third monitor, etc...). The position of each component relative to the line between the endpoints of the initial and final monitors may then be backed out by a simple calculation (illustrated in Fig. 10 and detailed below). Since the errors arising from each measurement are propagated across this system, its resolution is somewhat degraded (vs. the stretched-wire technique, where every sensor independently references a common wire). The major contributor to the sensor error over these short path lengths (assuming that thermal gradients are limited) is mechanical error in the mounting of the optical components. This may be reduced to applicable levels by positioning each element precisely in gauge blocks (as was performed at L3, and realized a resolution on the order of 6 μm[12]). Investigations have been performed by members of the SDC collaboration[8] into precision mounting of a light source and photosensor directly onto a lens, which can then be mechanically located by a precision mount. Although such a technique may involve considerable development and expense, it is a compact means of realizing nested monitor systems as shown in Fig. 10.

The offsets of the monitor components relative to the line connecting the endpoints may be derived by inverting a sparse matrix, as illustrated below for a 4-chamber (thus 3-monitor) system, as in Fig. 10.

11) $\Delta \mathbf{x} = \mathbf{b}\,([\mathrm{I}] - [\mathrm{A}])^{-1}$ *where:* [I] = 5 x 5 Identity

$$\mathbf{b} = \begin{bmatrix} 0 \\ \psi_2 \\ \psi_3 \\ \psi_4 \\ 0 \end{bmatrix} \qquad [\mathrm{A}] = \begin{bmatrix} 0 & 0 & 0 & 0 & 0 \\ \frac{\Delta z_{12}}{\Delta z_{13}} & 0 & \frac{\Delta z_{12}}{\Delta z_{13}} & 0 & 0 \\ 0 & \frac{\Delta z_{23}}{\Delta z_{24}} & 0 & \frac{\Delta z_{23}}{\Delta z_{24}} & 0 \\ 0 & 0 & \frac{\Delta z_{34}}{\Delta z_{35}} & 0 & \frac{\Delta z_{34}}{\Delta z_{35}} \\ 0 & 0 & 0 & 0 & 0 \end{bmatrix}$$

The calculation of Eq. 11 is performed independently for x and y coordinates (and is illustrated above for Δx). The vector **b** contains the measurements of the composite straightness monitors (as shown schematically in Fig. 10); since the Δx values are assumed to be relative to a common line between endpoints 1 and 5, the top and bottom components of **b** are zero. The matrix A specifies the monitor geometry. Its elements are

fixed (hence the inversion need only be calculated once), and essentially specify the spacing between the monitor components (of course, as the chambers deflect, the monitor spacing changes, injecting a small error, as discussed earlier). The simulation software emulates each composite monitor string via Eq. 1, and calculates the Δx deflections via Eq. 11. No difference is seen (using this limited model) from the stretched wire results as calculated by Eq. 10.

The layout of Fig. 10 assumes that at least two nested monitor systems run along each edge of each chamber; one (upper in figure) to measure the offset of the rightmost chamber corners, and another (lower in figure) to measure the offset of the leftmost chamber corners. This technique, while attractive mechanically (i.e. the fragility and complication of a stretched wire is avoided), is not readily amenable to including interim references placed along a chamber frame (perhaps useful for cathode strip devices).

The multipoint schemes of Figs. 9 & 10 will produce a Δx and Δy value at each chamber corner. During the reconstruction procedure, these must be interpolated (linearly in the current scheme) between the 4 endpoints of each chamber traversed by a muon, at the position of the muon intercept (as measured in local chamber coordinates). This correction is then added into the muon spacepoints for each superlayer (thus referencing them to the lines between superlayer edges). These are then adjusted by the results of the inter-layer 3-point monitors, first interpolated along the z-axis. A linear interpolation (expressed in terms of cot θ) is performed on the quadratic coefficients (A,B,C; see Eq. 6) determined by the 90° and 30° monitors, at the angle θ specified by a least-squares fit between the 3 superlayer spacepoints. The resulting quadratic coefficients are used to interpolate across tan ϕ (using the coordinates of the muon intercept on the middle superlayer, corrected as described in Eq. 7).

2) Simulation Results

The alignment scheme described in the previous section has been simulated for a single barrel hexant (i.e. Fig. 1) using the MATLAB interpreter package[13] running on a Macintosh Quadra 700. MATLAB has several advantages over standard languages such as FORTRAN; i.e. implicit matrix/vector formalism, simple access to a wide variety of efficient numerical routines, interactive graphics, and an intuitive approach to debugging and development. There were a few drawbacks to this application, however; i.e. no capability in the current MATLAB release to easily define arrays of matrices, and the slow speed of the interpreter (which was not too inconvenient when running on the Quadra).

The software was set up so that rotations (about local x,y,z axes), translations (x,y,z), and scalings (x,y,z) could be independently specified as matricies (i.e. as performed in Ref. [14]) for each chamber, each superlayer, and globally for the entire hexant. These transformations were specified by 4 x 4 matrices in order to implicitly include translations, as is standard in computer graphics applications[15]. All transformations were concatenated into a single matrix for each chamber (first scalings are applied, then rotations, finally translations; the individual chamber transformations are applied first, followed by the superlayer transformations, and finally the global transformations).

Straight-line muons sweep the hexant in a raster scan of 40 (θ) by 11 (ϕ) points. The measured muon spacepoints are calculated by finding the intercept of the muon track with the transformed chambers, then transforming back (with the inverse matrix) to produce the intercept in local chamber coordinates. Uncorrected sagittas are calculated via. Eq. 3, then corrected by the simulated alignment monitors (as discussed above), and calculated again. The uncorrected sagittas, correction function, and corrected sagittas are mesh-plotted vs. θ and ϕ. In addition, slices are plotted through the uncorrected and corrected sagittas at $\theta = 90°, 60°, 30°$ (vs. ϕ) and at $\phi = -11.25°, 0, +11.25°$ (vs. θ).

The simulated stretched-wire system is used to correct the chamber positioning along the z-axis. These measurements are displayed in a set of plots (together with the measurements derived from the nested monitor systems, which were seen to be identical). A final group of plots shows the measurements from the projective, inter-superlayer 3-point monitors.

The superlayer configuration (Fig. 1) is structured in rough accordance with the GEM Baseline II specification. The outer layer (#3) is assumed to contain 4 chamber packages at y = 8700 mm from the beamline, the middle layer (#2) contains 3 chamber packages at y = 6310 mm, and the inner layer (#1) contains 2 chamber packages at y = 3920 mm. All chamber packages are sized identically in z and projectively in x.

The first example is exceedingly straightforward; i.e. all chambers in the middle superlayer are translated along the bending coordinate (x) by 10 mm (see Fig. 3). Fig. 11 shows the raw and corrected sagittas. It is immediately evident that the measurements from the straightness monitor system perfectly reproduce the muon measurements, hence completely annihilate the sagitta error, which is constant in θ and ϕ. The straightness monitor measurements (as projected onto the chamber planes by dividing by the cosine of their inclination; see Sec. 1) are plotted in Fig. 12; the Δx shift is directly detected at all 3-point sensor locations (the deflection along x couples into the Δy measurement seen by the projective monitors at $\theta = 30°$). Since individual chambers are not displaced in this

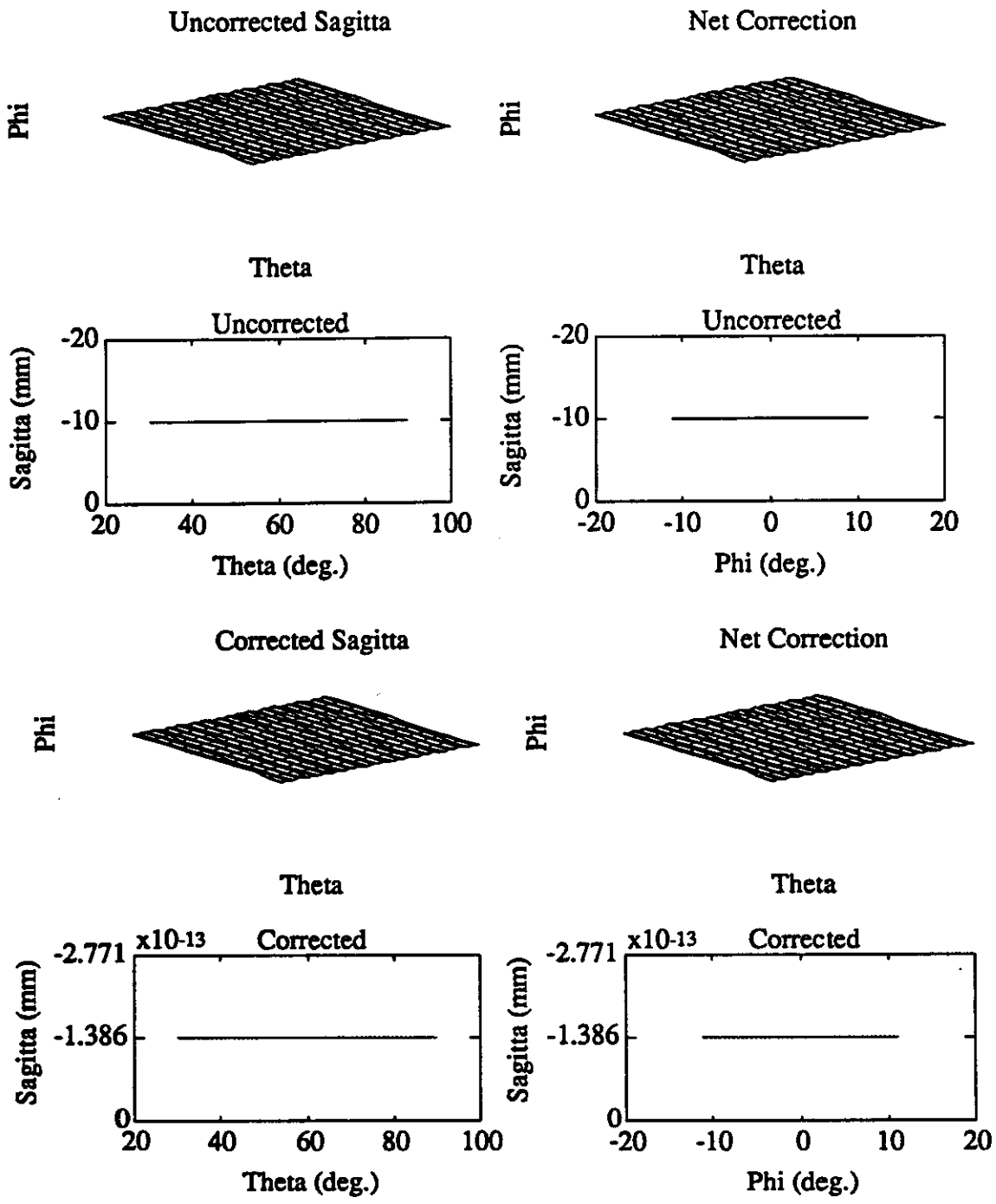

Figure 11: Sagitta error and correction for middle superlayer offset by Δx = 10 mm

example, the multipoint measurements are zero all along the superlayers, as seen in the lower sets of plots in Fig. 12 (these plots will thus be omitted in all tests excepting those that displace individual chambers).

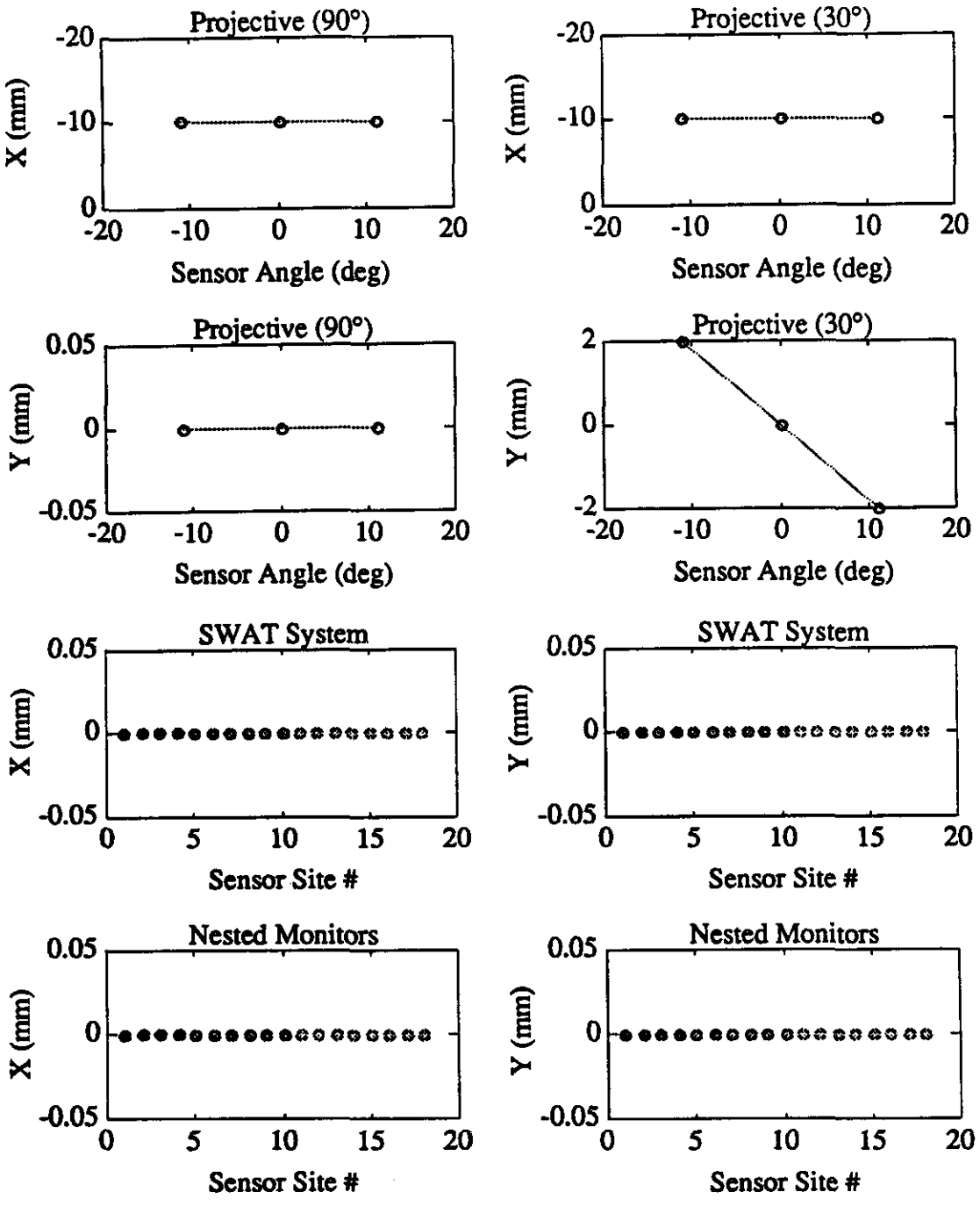

Figure 12: Straightness monitor measurements for middle superlayer offset by Δx = 10 mm

The next example is as well a translation in x, however now the outer superlayer (#3) is shifted by Δx = 20 mm (see Fig. 4). Sagittas and corrections are shown in Fig. 13. Due to the rotation of the projective alignment axes, the monitors running at opposite sides of the hexant in ϕ see slightly different sagittas (which are not encountered by the straight-line muon). This is evident in the curve of the correction, which is caused by a

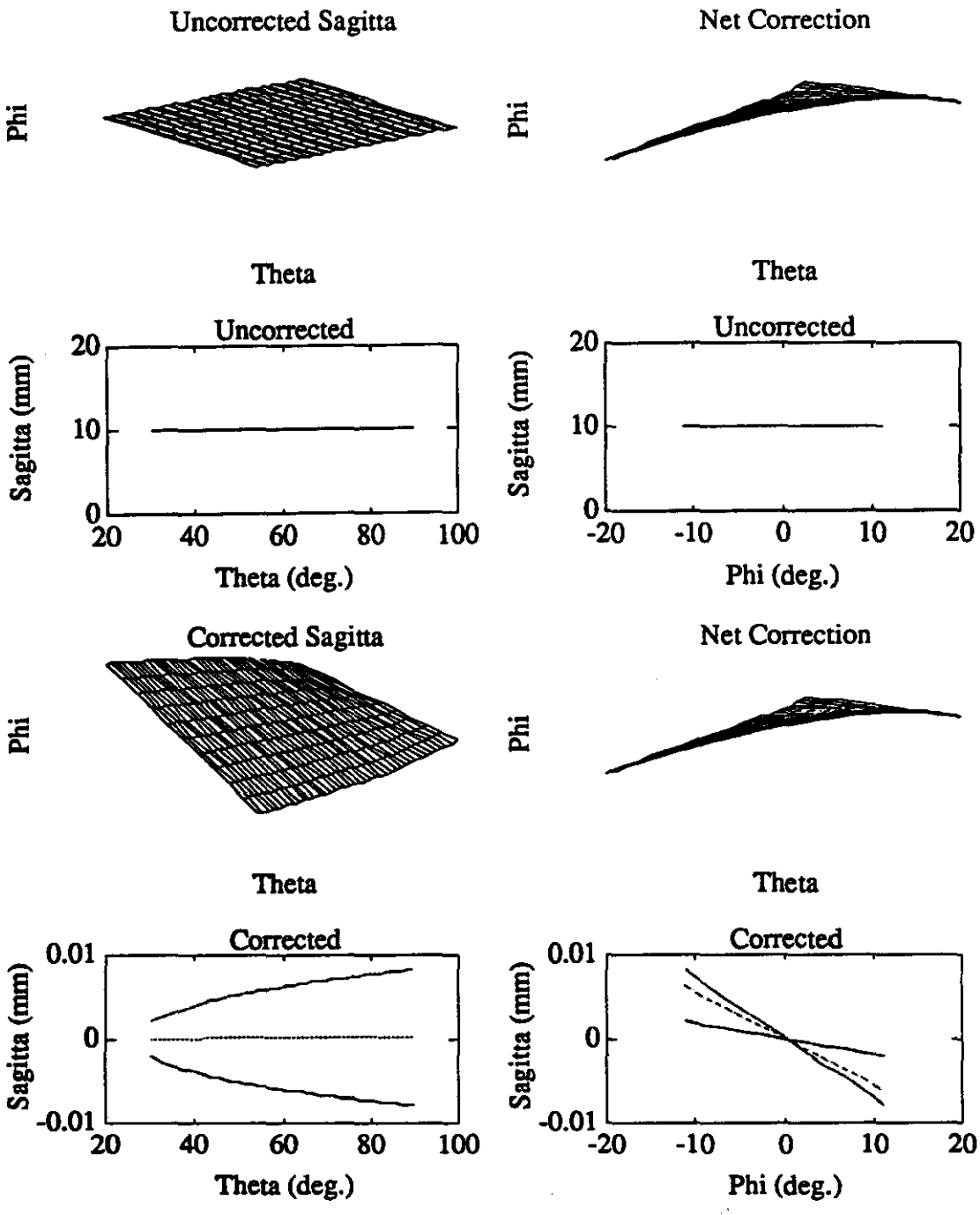

Figure 13: Sagitta error and correction for outer superlayer offset by $\Delta x = 10$ mm

small quadratic component arising from the monitor mismatch, producing an analogous residual error, approaching 10 μm at the superlayer edges (larger at $\theta = 90°$). The projective monitor measurements are given in Fig. 13. The small difference between the monitors at opposite ϕ angle can not be discerned here, thus a table output from the simulation has been included to list these results (which disagree by 4 μm, front-to-back).

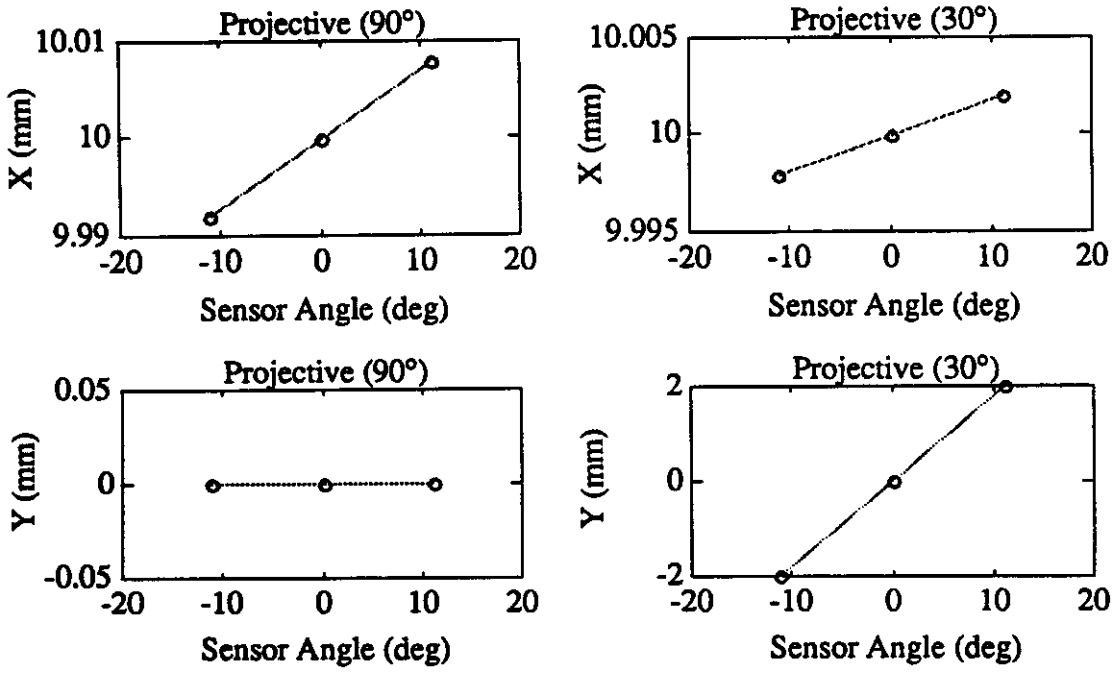

Monitor Corrections

```
Radial monitors at 90°
x_front (mm):    9.9918  |  x_mid (mm):    9.9998  |  x_back (mm):   10.0078
z_front (mm):    0.0000  |  z_mid (mm):    0.0000  |  z_back (mm):    0.0000
Radial monitors at 30°
x_front (mm):    9.9979  |  x_mid (mm):   10.0000  |  x_back (mm):   10.0020
y_front (mm):   -1.9887  |  y_mid (mm):    0.0000  |  y_back (mm):    1.9895
-------------------------------------------------------------

Quadratic Coefficients:
90° Monitors: A =   0.0005   B =   0.0402   C =   9.9998
30° Monitors: A =   0.0000   B =   0.0104   C =   9.9999
```

Figure 14: Straightness monitor measurements for outer superlayer offset by Δx = 10 mm

The next example applies a scale factor to the x-dimension of the middle chamber layer (see Fig. 6 and discussion). The measured x-coordinate is effectively reduced by a factor of 0.995. Sagittas and corrections are given in Fig. 15, while the straightness monitor measurements are plotted in Fig. 16. Although the straightness monitors detected roughly 6.3 mm of sagitta error, a residual remains after correction, approaching 50 μm at the chamber edges!

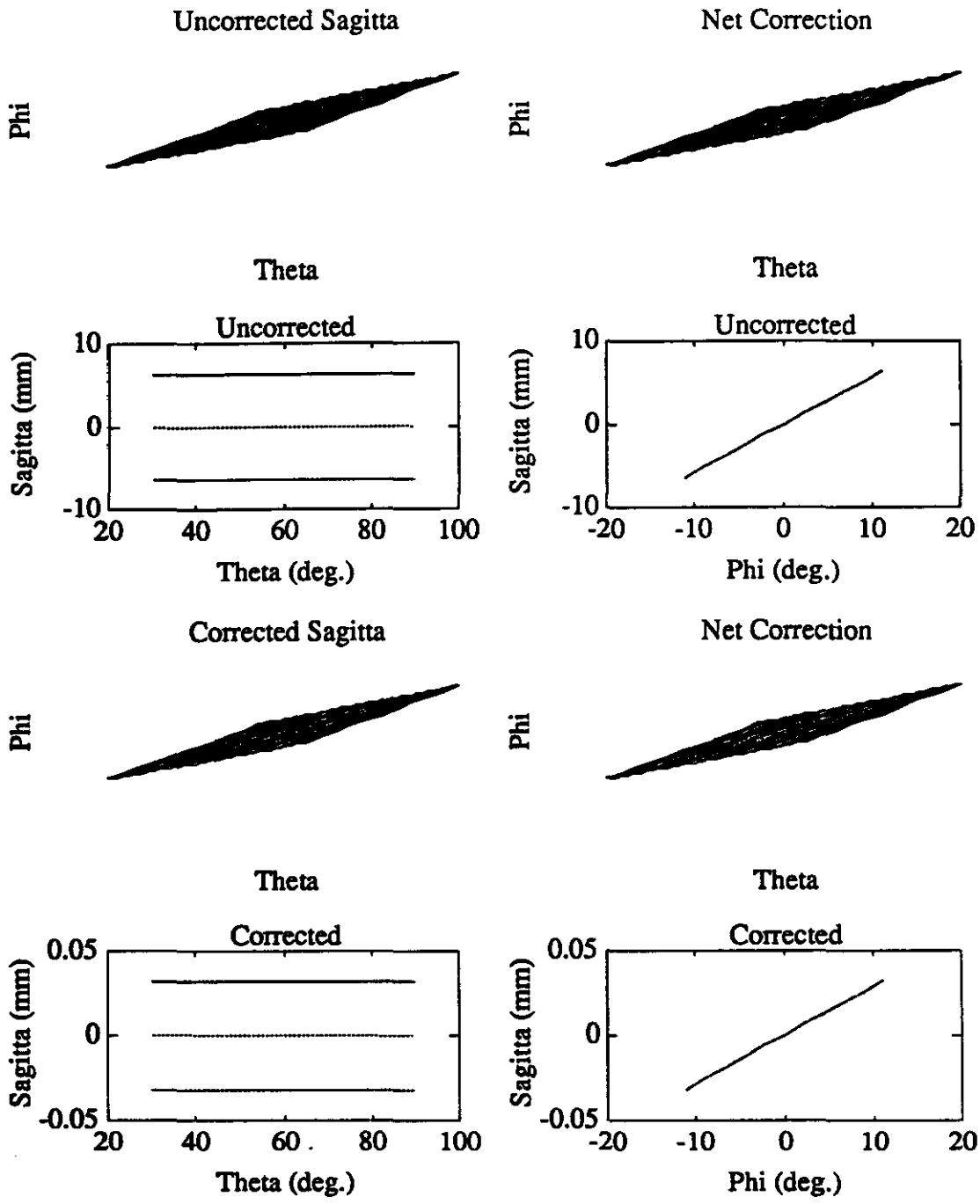

Figure 15: Sagitta error and correction for middle superlayer x-coordinate scaled by 0.995

This is due to the addition of the sagitta error into the fit ordinates (as in Eq. 7), and was discussed at length for Fig. 6. Although this correction aids in compensating Δy error, it generates susceptibility to scaling errors, such as noted here.

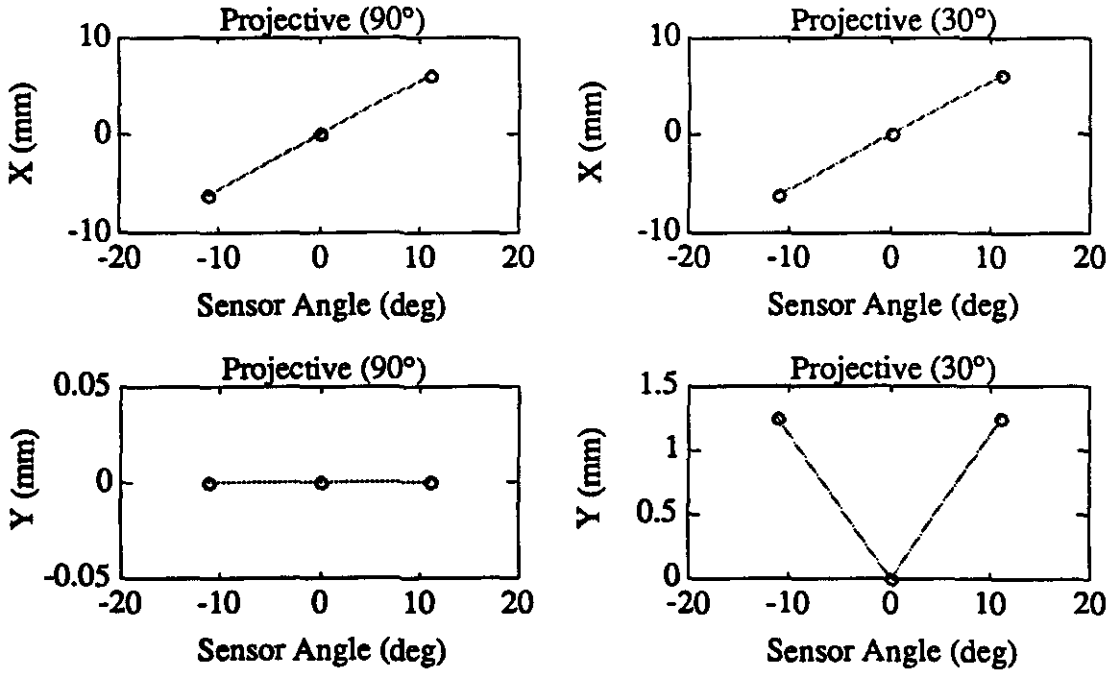

Figure 16: Projective monitor measurements for middle superlayer x-coordinate scaled by 0.995

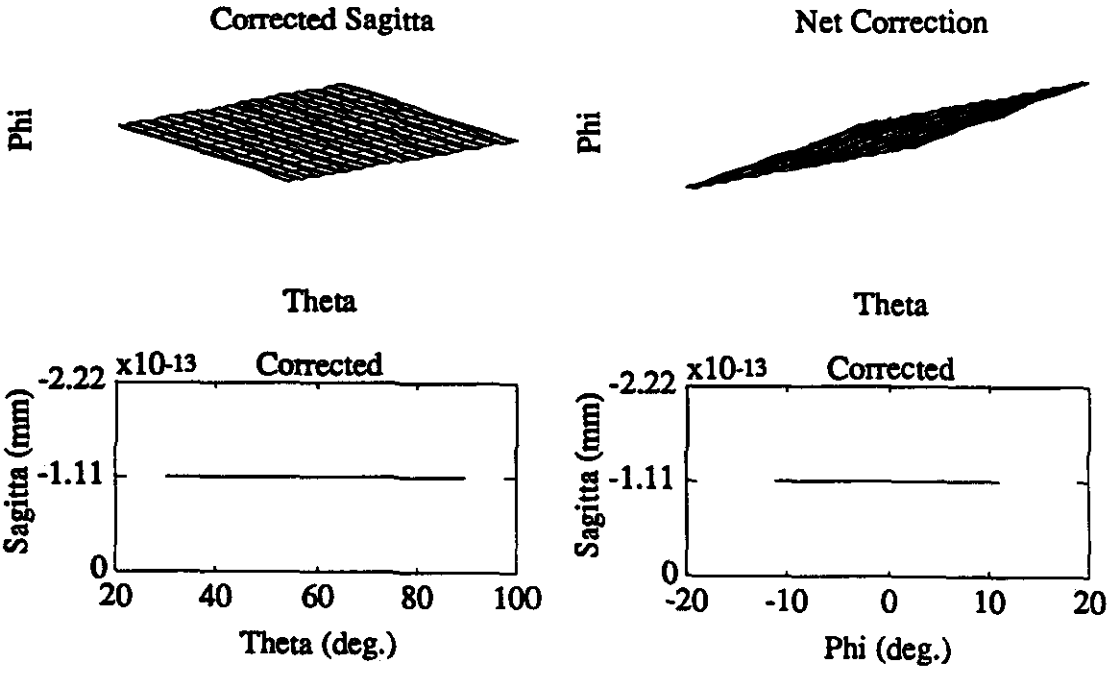

Figure 17: Sagitta residual for middle superlayer x-coordinate scaled by 0.995; no fit correction

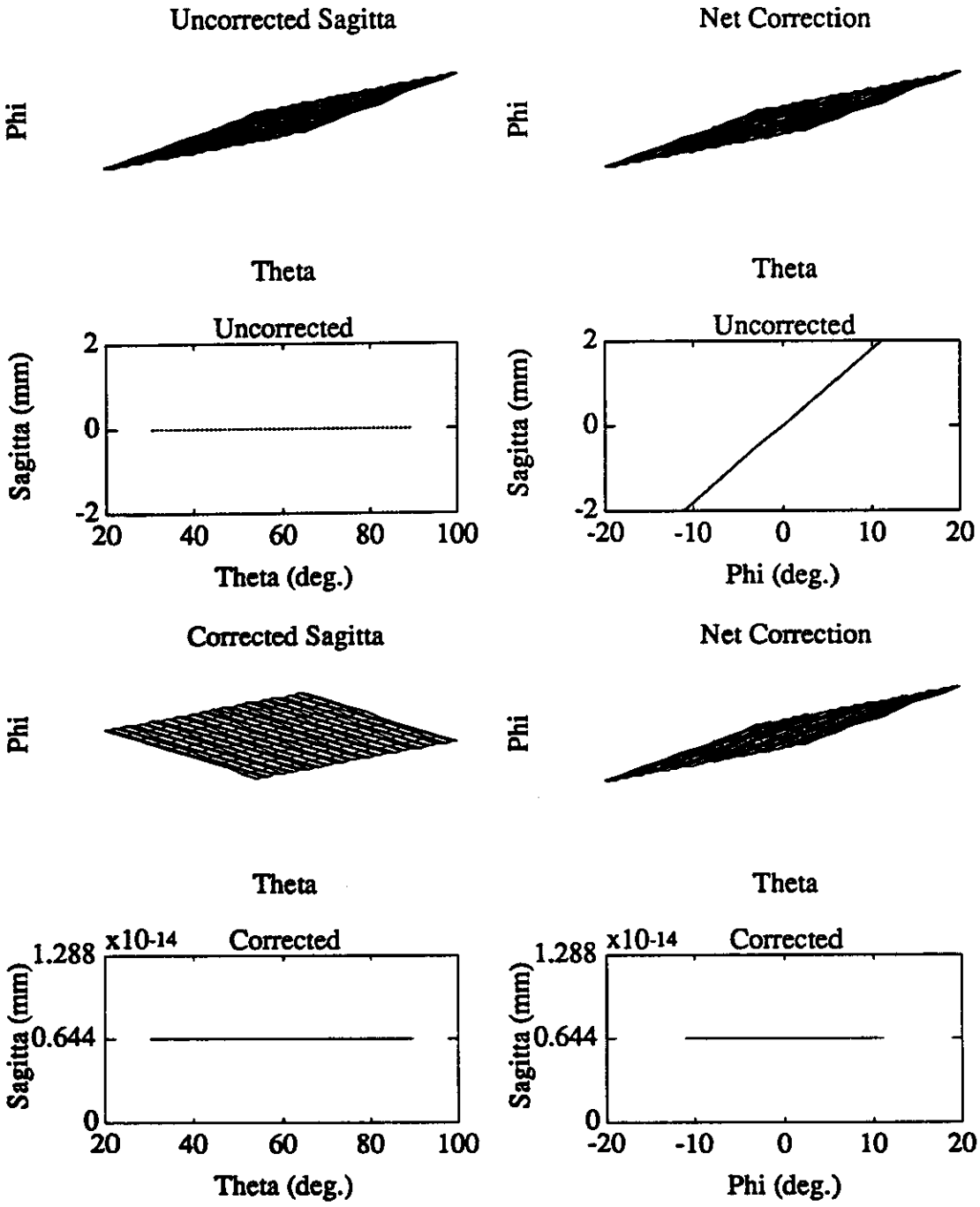

Figure 18: Sagitta error and correction for middle superlayer radially offset by Δy = 10 mm

Fig. 17 shows the same chamber deformation (x scaling by 0.995) as in Fig. 15, however here the ordinate corrections of Eq. 7 have been omitted. Indeed, the sagitta error is now fully compensated. In order to retain consistency, however, all examples in this report employ the correction of Eq. 7, unless explicitly stated otherwise.

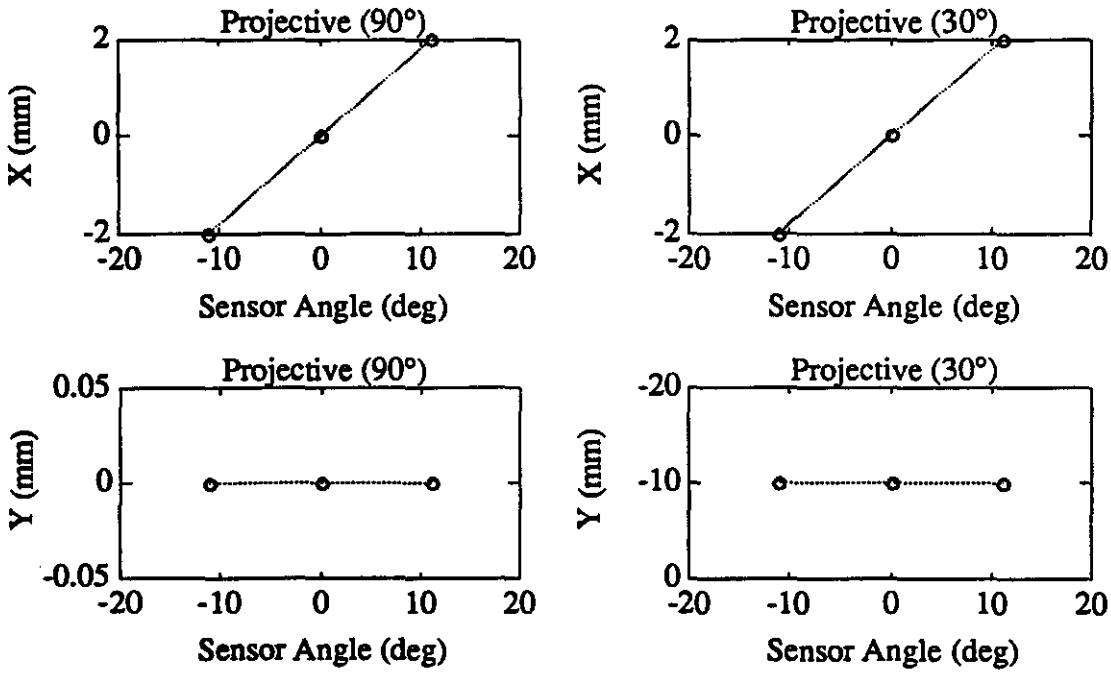

Figure 19: Projective monitor measurements for middle superlayer radially offset by Δy = 10 mm

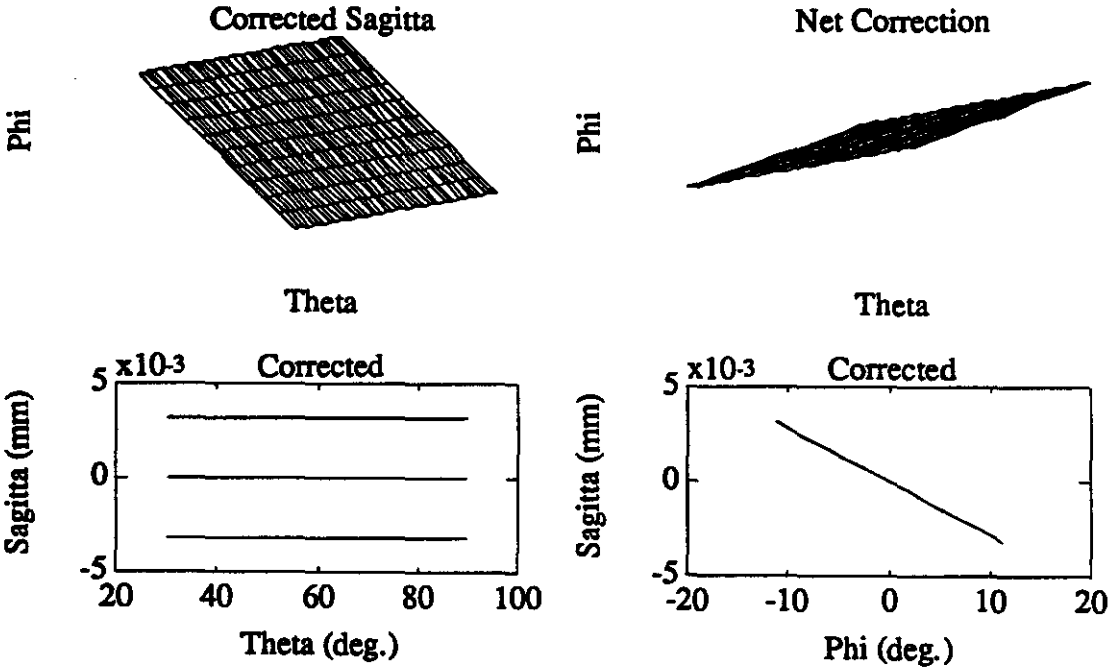

Figure 20: Sagitta residual for middle superlayer radially offset by Δy = 10 mm; no fit correction

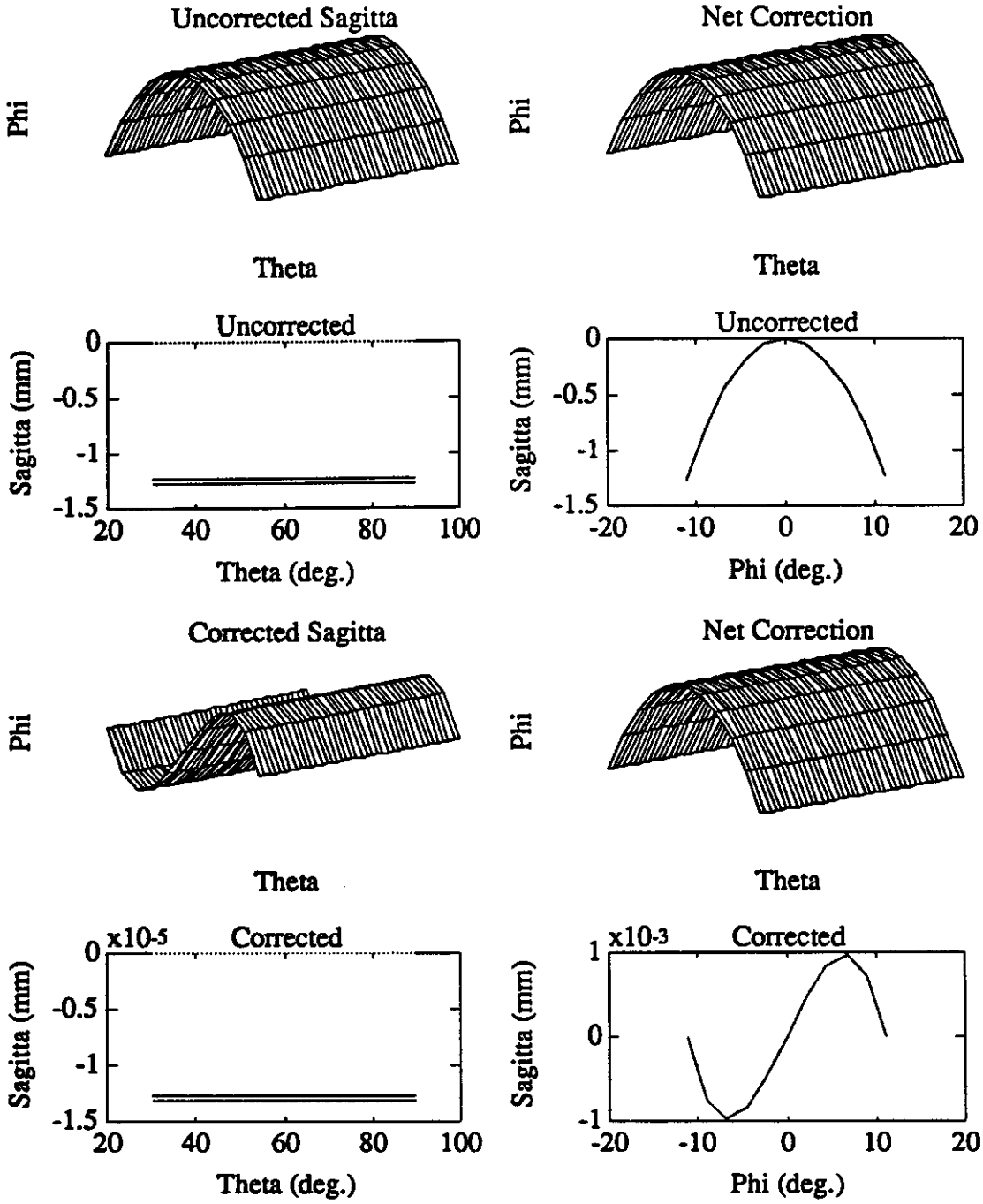

Figure 21: Sagitta error and correction for middle superlayer rotated by 5 mr about z-axis

The next example applies a simple radial offset of the middle superlayer (as depicted in Fig. 5) of $\Delta y = 10$ mm. The sagitta and corrections are shown in Fig. 18. The error is seen to be essentially linear in ϕ, reaching up to ± 2 mm. The straightness monitors, which are seen to properly measure the superlayer positioning in Fig. 19, apply a perfect cancellation.

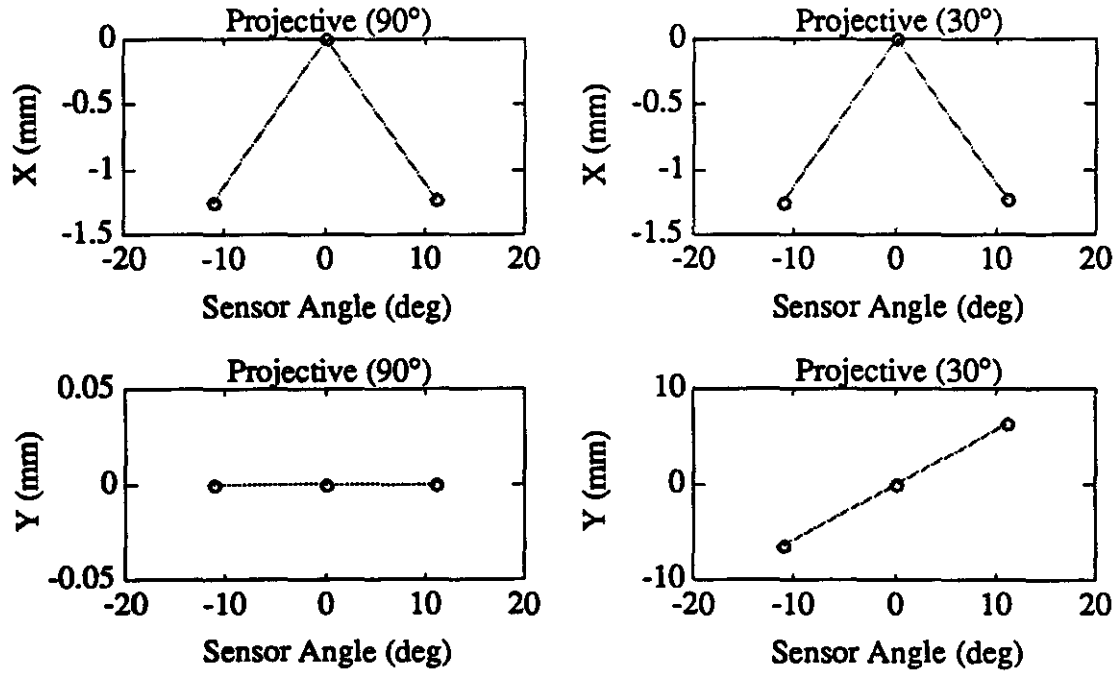

Figure 22: Projective monitor measurements for middle superlayer rotated by 5 mr about z-axis

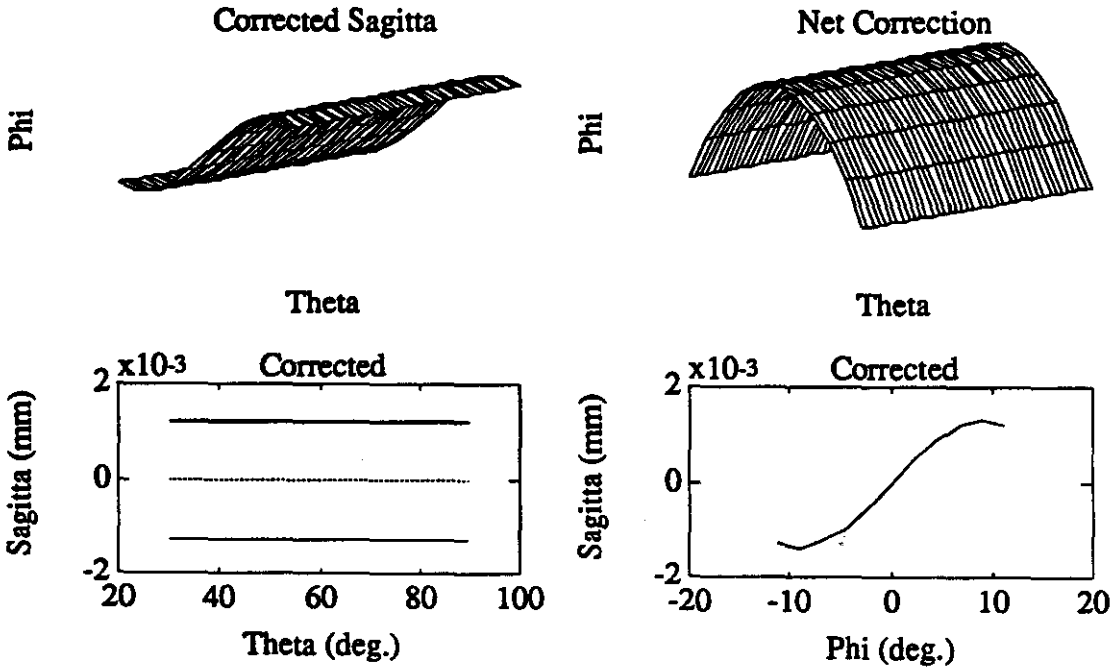

Figure 23: Sagitta correction and residual for middle superlayer rotated by 5 mr about z-axis; no second-order correction included

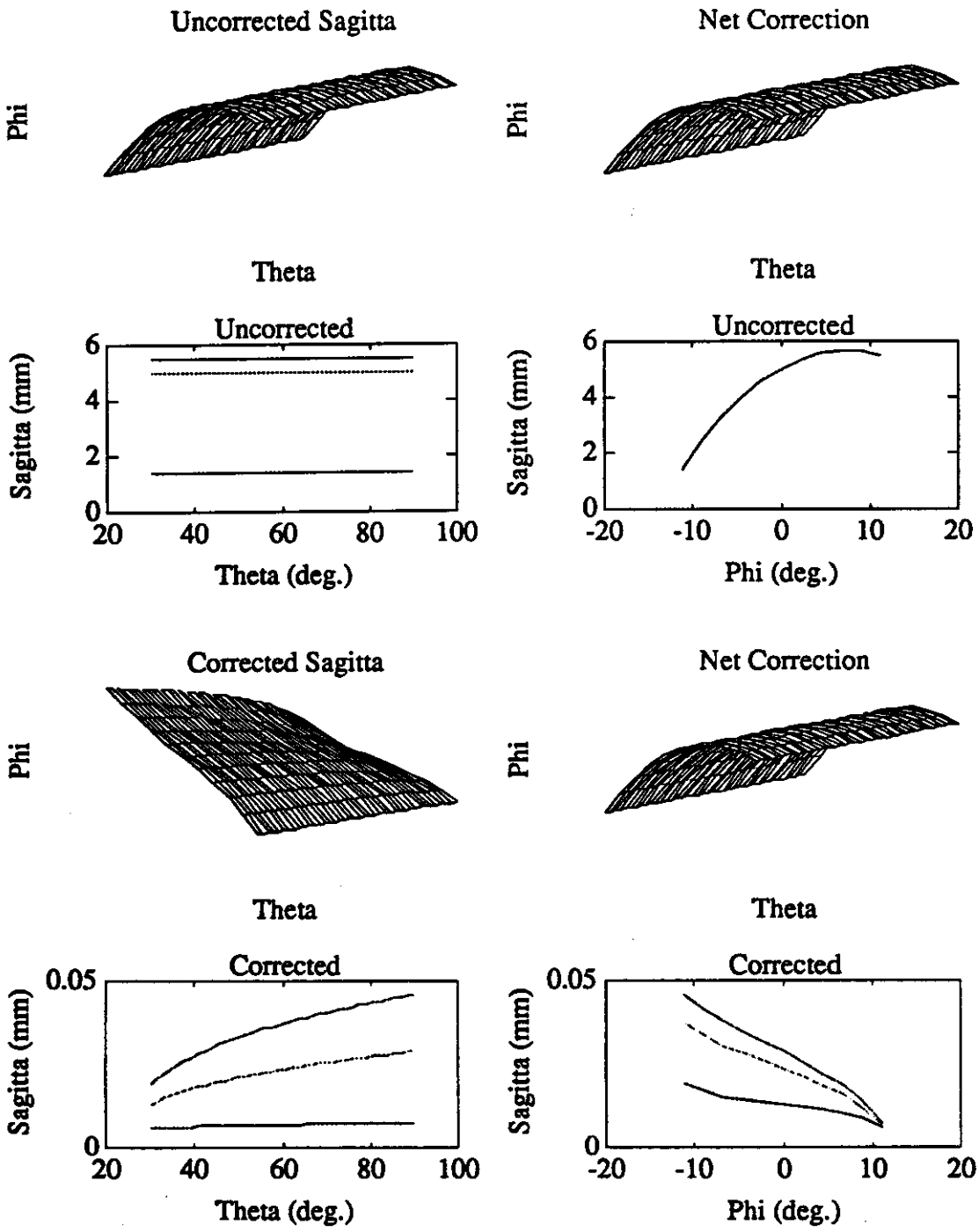

Figure 24: Sagitta error and correction for various z rotations & superlayer translations

Fig. 20 shows the sagitta correction and residual for the same chamber displacement, except the ordinate correction of Eq. 7 is omitted. The error cancellation is no longer perfect, and residuals of up to 5 μm are noted at the hexant edges.

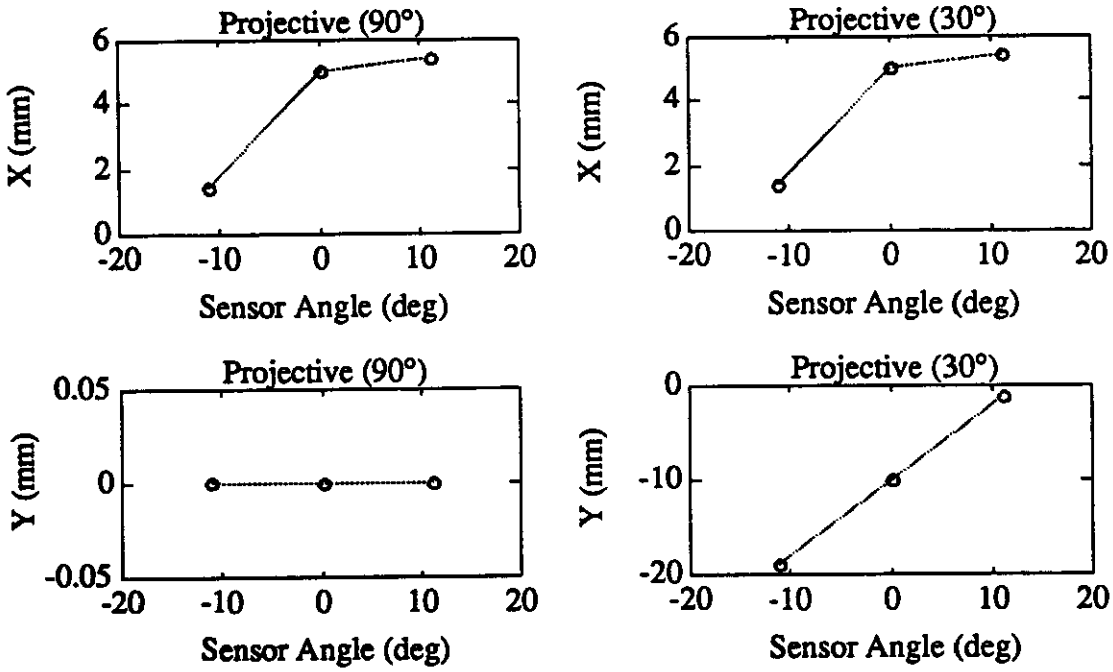

Figure 25: Projective monitor measurements for various z rotations & superlayer translations

As expected, chamber offsets along the z-axis have been seen to create no sagitta error or produce finite corrections from the alignment monitor measurements, hence z-offset examples are not presented in this report.

The next example examines a rotation of the middle chamber about the z-axis (see Fig. 7) by 5 milliradians. Fig. 21 shows the sagitta error, correction, and residual. The quadratic nature of the sagitta error is obvious. The maximum error of 1.5 mm is reduced to under 1 μm by the alignment correction (monitor outputs are shown in Fig. 22), which leaves a residual appearing somewhat sinusoidal. Fig. 23 shows the alignment correction and residual for the same example, except now the second-order ordinate correction of Eq. 8 is omitted. The improvement is modest; the residual now extends to nearly 2 μm at the hexant edges. Note that the results with the second-order correction (Fig. 21) gave a zero residual at the location of the alignment monitors, indicating a proper compensation at the position where the measurements are taken.

The next example combines the above tests, in that several superlayers are simultaneously rotated about z and translated along various axes. In particular, layer 2 is rotated by 5 mr about z, layer 1 is rotated by -4 mr about z, layer 1 is offset by 10 mm in x, and layer 2 is offset by 10 mm in y. Sagitta effects and corrections are shown in Fig. 24. The initial error of up to 6 mm is compensated by the monitor systems (Fig. 25) down to the 50 μm level, with the residual showing significant θ dependance (probably due projective errors in the monitor systems).

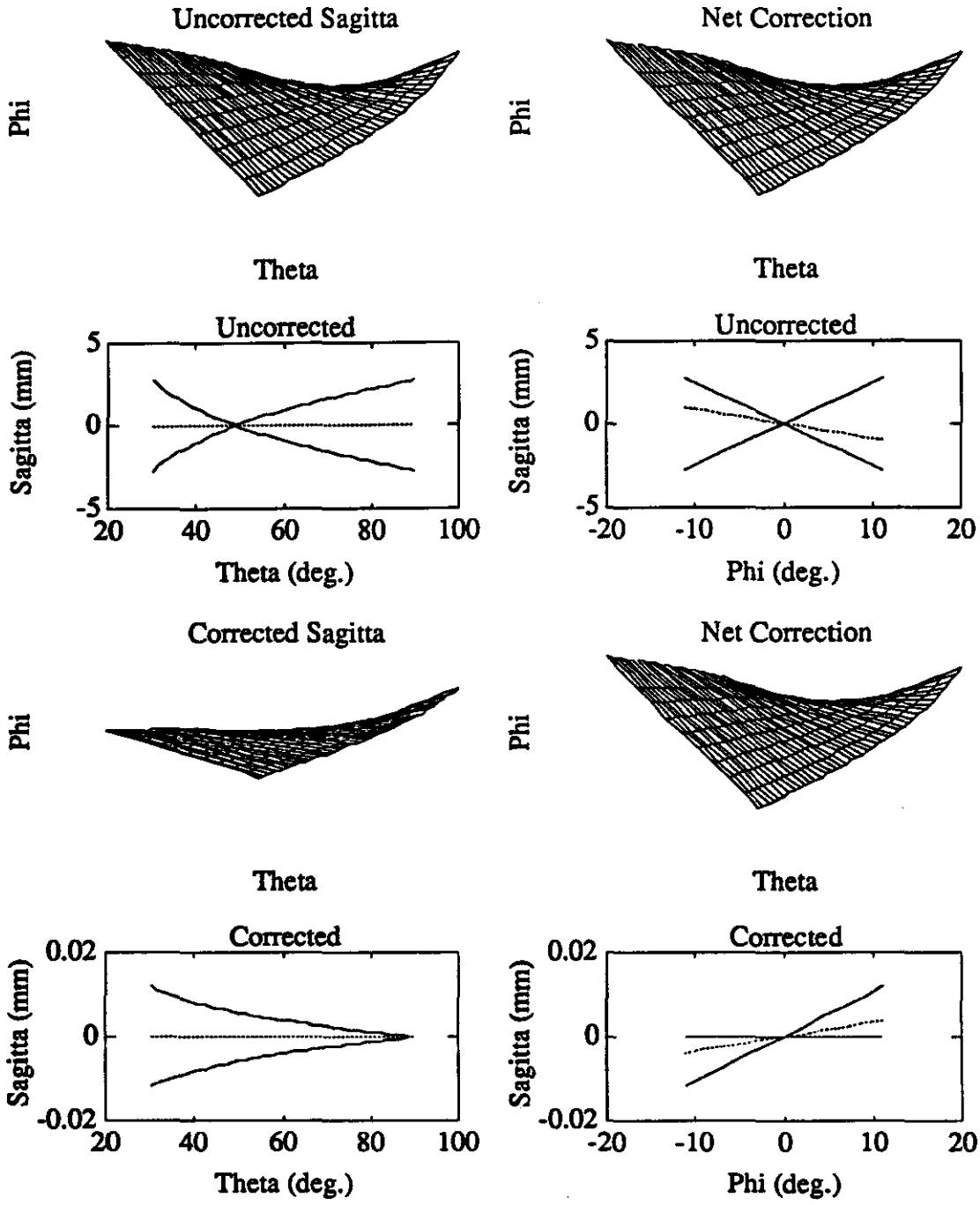

Figure 26: Sagitta error and correction for rotation of middle superlayer by 2.5 mr about the x-axis

In the next example, the middle superlayer is rotated by 2.5 milliradians about the x-axis. Sagitta results are shown in Fig. 26, where we see a maximum error of roughly 3 mm produced at the θ extremes of the hexant. These are appreciably attenuated by the correction from the monitor measurements (Fig. 27), although significant residuals of up to 15 μm remain, depending on θ and ϕ.

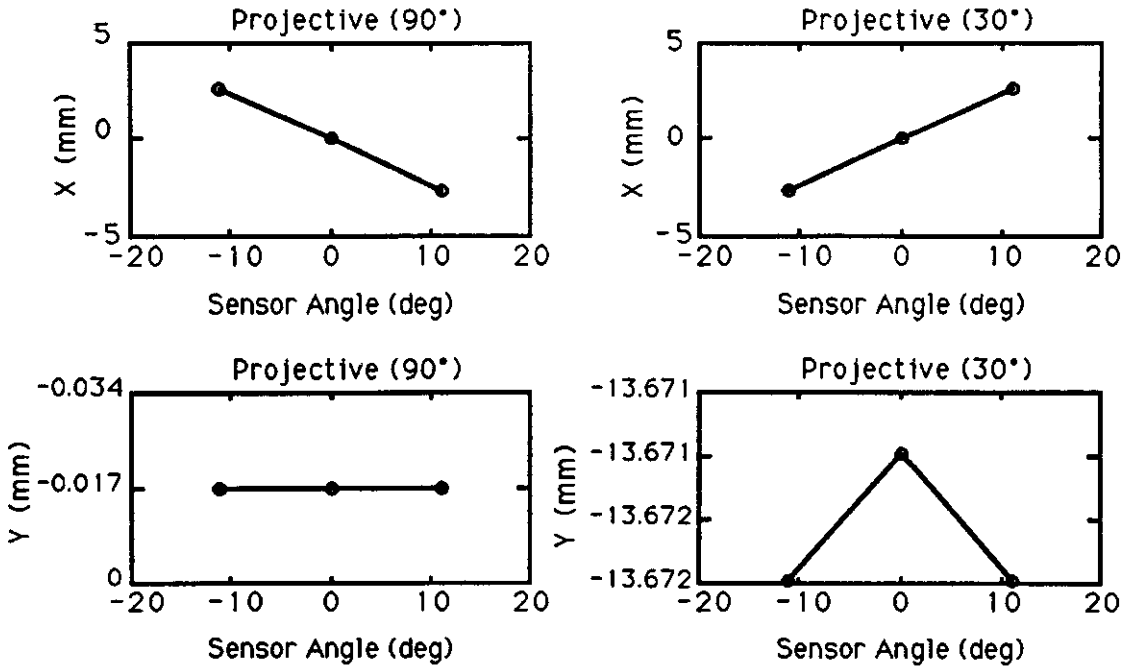

Figure 27: Projective monitor measurements for rotation of middle superlayer by 2.5 mr about x-axis

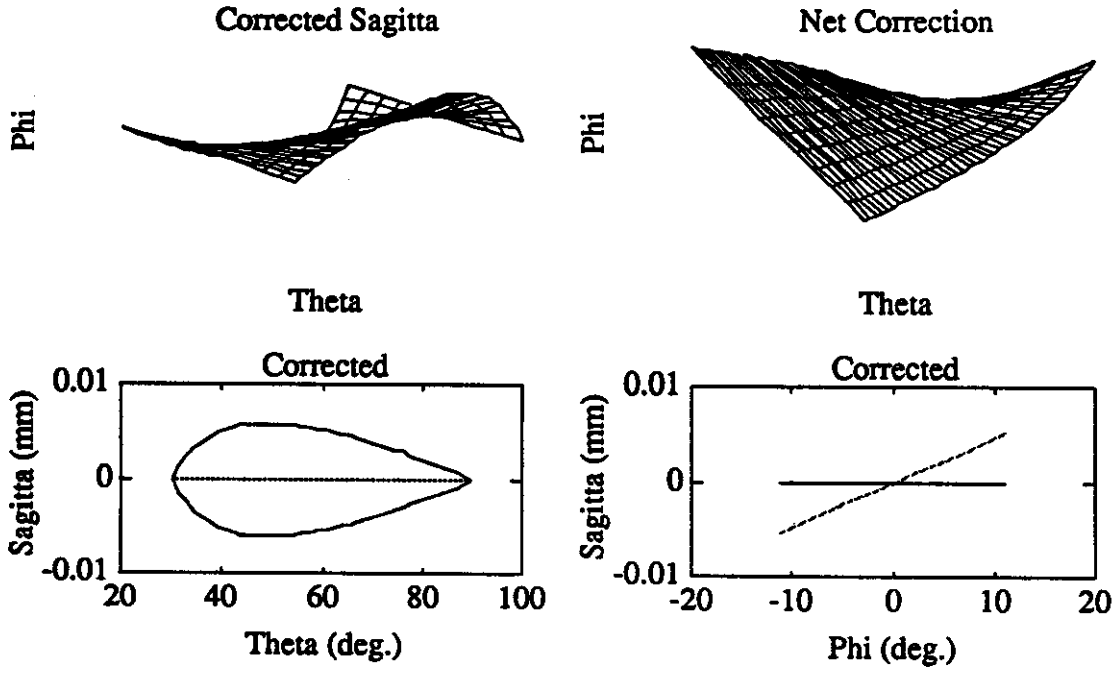

Figure 28: Sagitta residual and correction for rotation of middle superlayer by 2.5 mr about x-axis; "ideal" z-coordinate correction applied

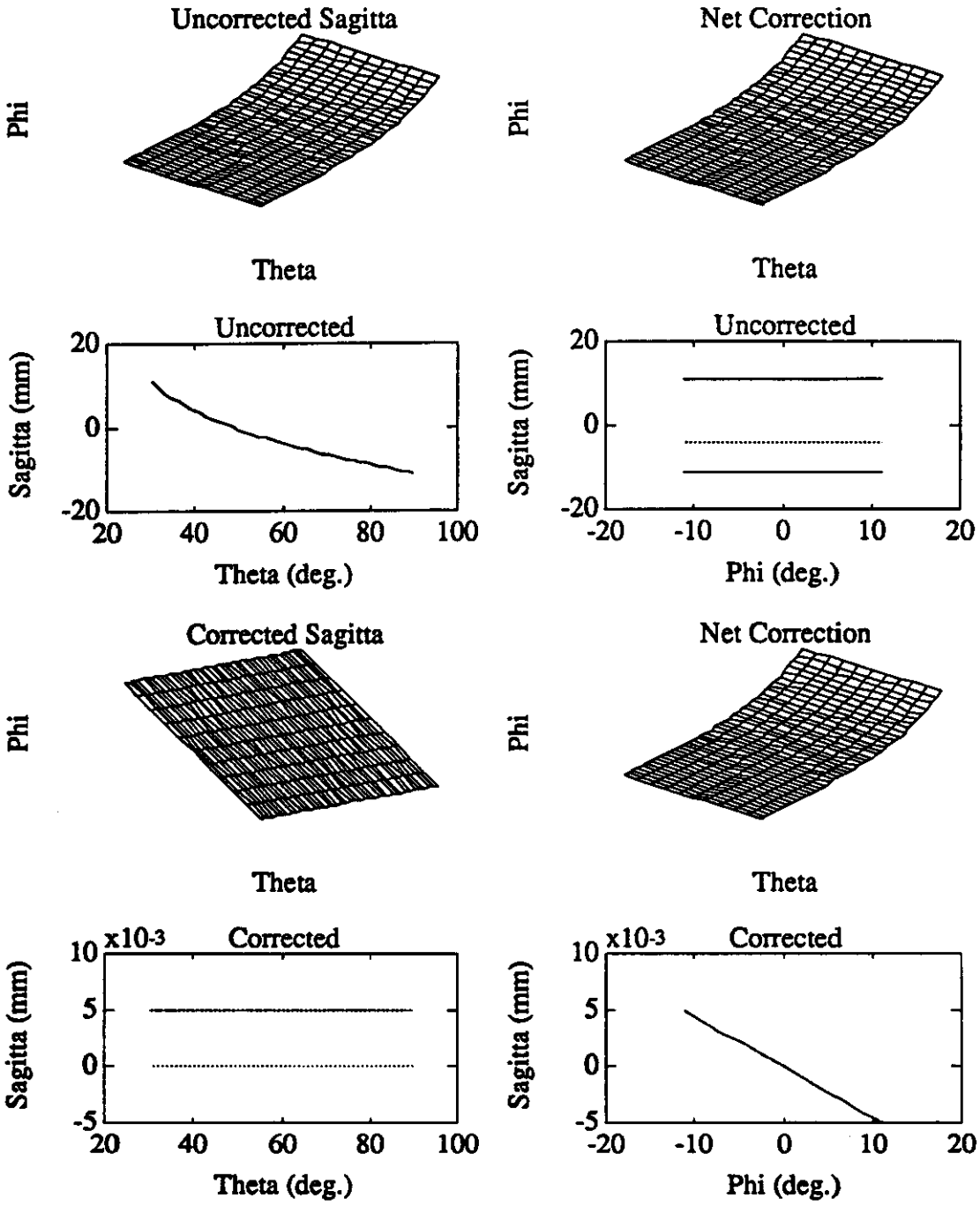

Figure 29: Sagitta error and correction for rotation of middle superlayer by 2.0 mr about the y-axis

Much of this error is due to problems implicit in the z-interpolation, as discussed in the first section of this report. Fig. 28 shows the residuals for the same example, except the z-sagitta is now corrected by "perfect" chamber measurements; the worst-case sagitta residual has been reduced by better than a factor of two. Note that the residual at the monitor locations is zero here, and all remaining error is in the interpolation.

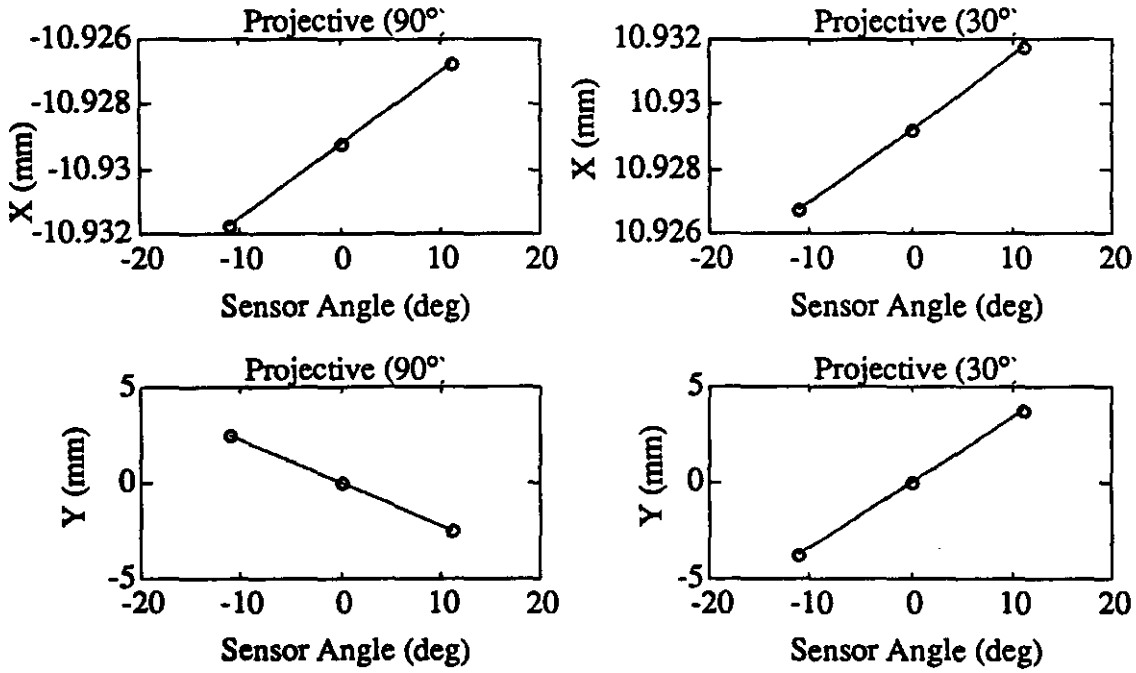

Figure 30: Projective monitor measurements for rotation of middle superlayer by 2.0 mr about y-axis

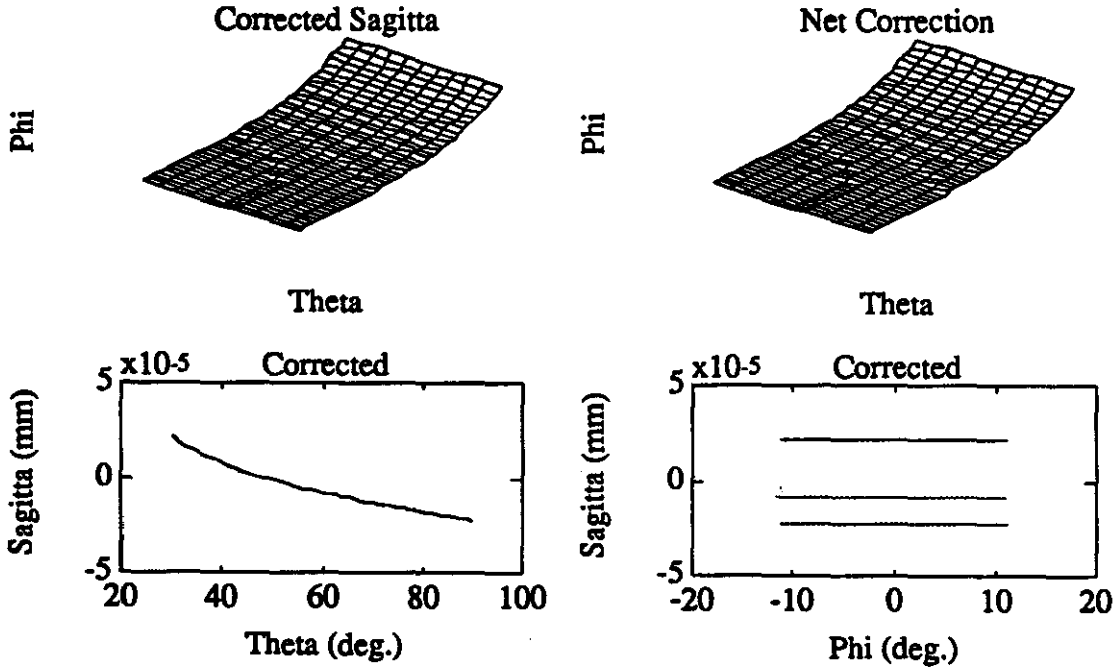

Figure 31: Sagitta residual and correction for rotation of middle superlayer by 2.0 mr about y-axis; "ideal" z-coordinate correction applied

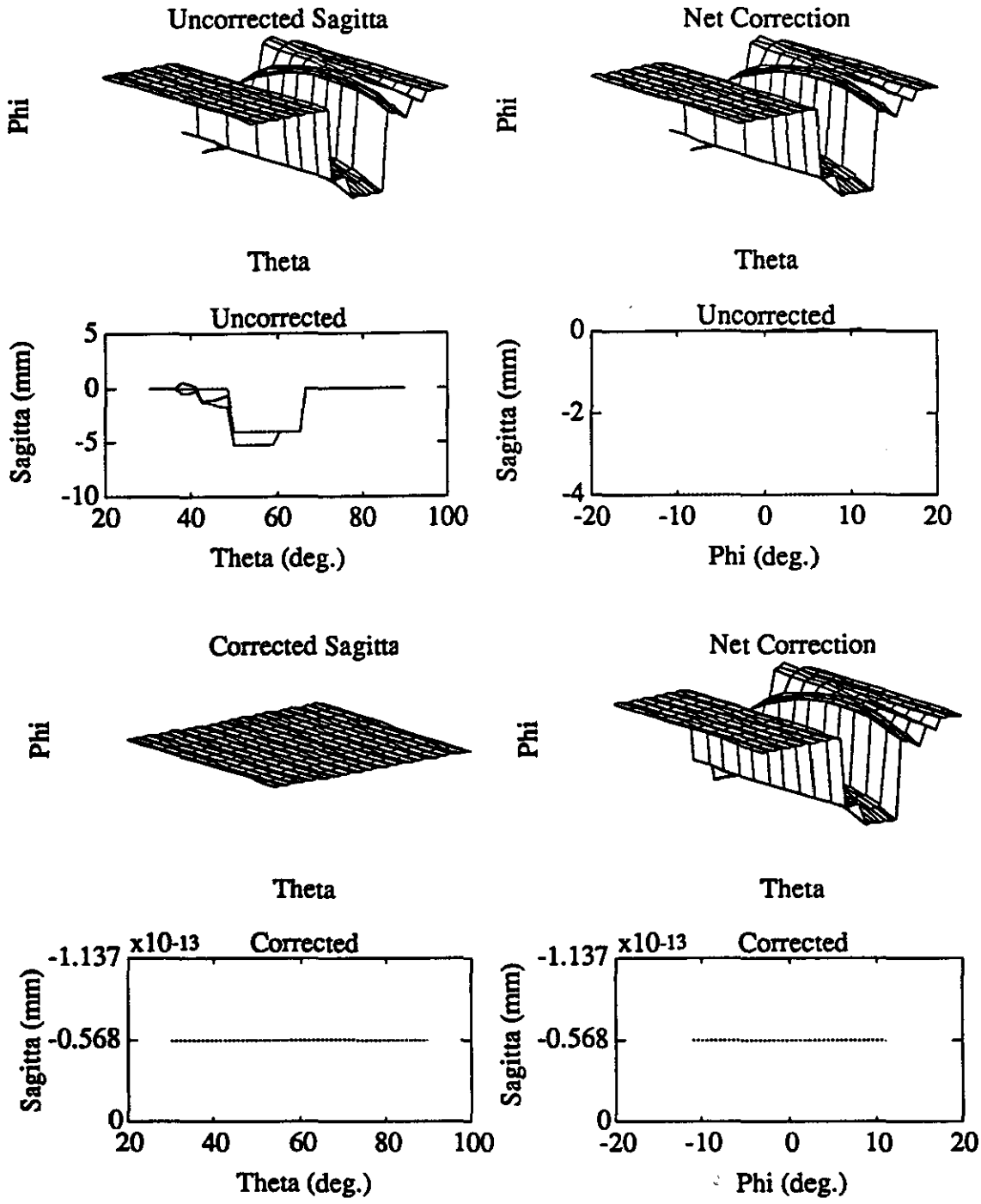

Figure 32: Sagitta error and correction for displacements of inner chamber packages

The ordinate correction of Eq. 7 does not aid in reducing sagitta errors from such x-rotations; if these corrections are omitted, the sagitta residuals in Fig. 26 are reduced by nearly half.

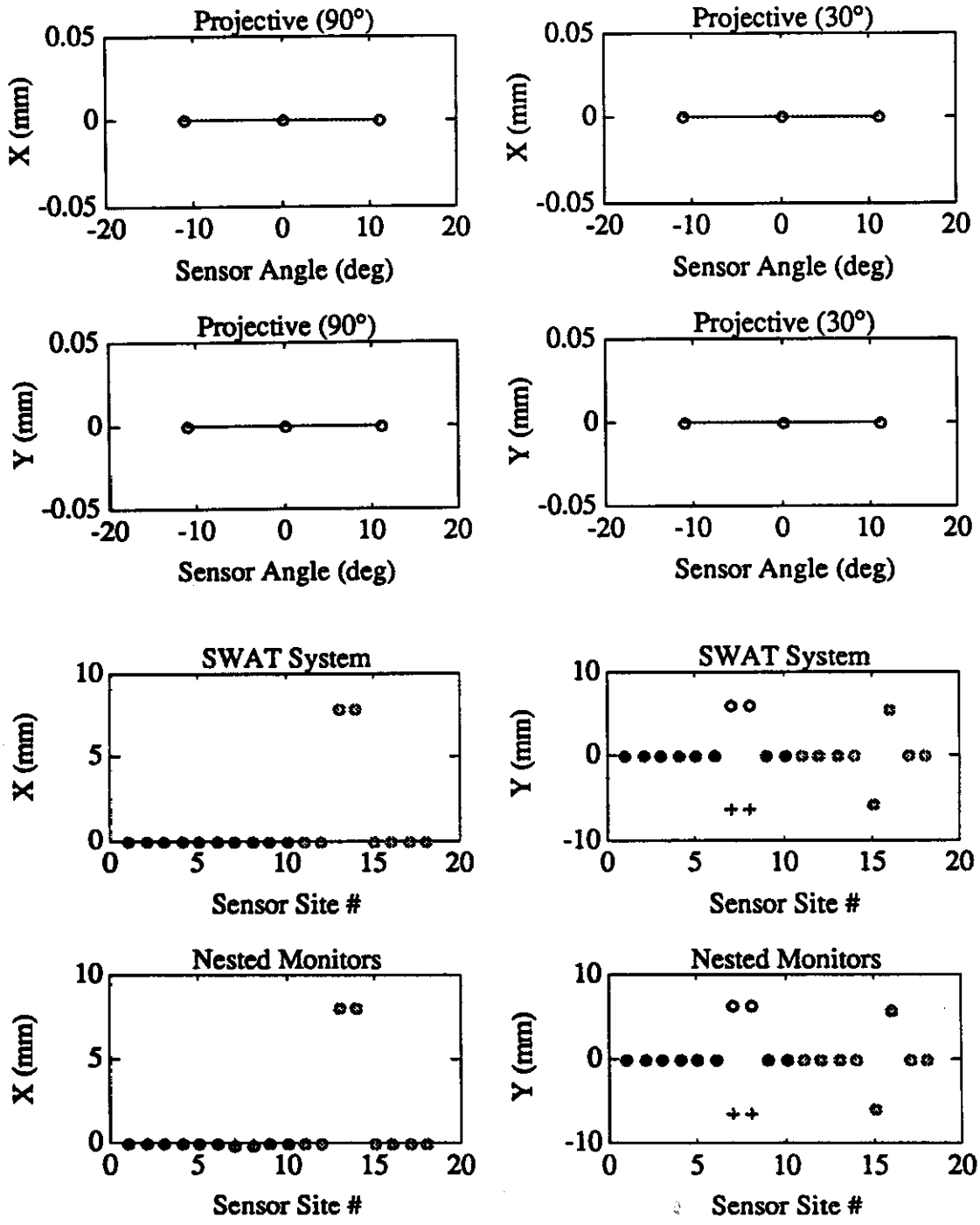

Figure 33: Straightness monitor measurements for displacements of inner chambers

The next example examines a rotation about the y-axis of the middle chamber layer by 2 milliradians. Figure 29 shows the sagitta results; we see a sizable position error created (on the order of 15 mm in the worst case), which is attenuated to the 5 μm level by the corrections from the alignment monitor measurements (Fig. 30). If z-axis

adjustments from "perfect" chamber resolution are also included, the chamber misalignment can be nearly perfectly corrected, as seen in Fig. 31. In contrast to the x-rotations shown in the previous set of examples, these y-rotations benefit from the ordinate corrections of Eq. 7 (again, on the order of 50% improvement has been realized in this example; Figs. 29,31 account for these correction).

The next example illustrates the performance of the multipoint monitors along the z-axis. A series of transformations (various translations and rotations) are applied to the chamber packages that do not move the projective monitors (i.e. the chambers at the θ edges of the hexants are not displaced, and no superlayer transformations are applied). Sagitta results are shown in Fig. 32. A complicated sagitta error function is realized (with peak amplitude approaching 5 mm) as the straight-line muons are swept across the various displaced chambers and their deflections are combined (since the chambers at the θ extremes remain undisturbed, the error is zero in these regions). As can be seen at the bottom of Fig. 32, this error is completely canceled by the multipoint monitor measurements. The Δx and Δy coordinates measured by the alignment system are able to completely describe the chamber misalignment (of course this is a simplified system; we assume that a set of monitors running on each chamber edge [i.e. $\phi = \pm 11.25°$] can be linearly interpolated into the chamber body; i.e. the chamber wire supports are perfectly rigid or uniformly scaled).

Since the projective monitors (top of Fig. 33) measure zero deflection, they introduce no correction in this example. The multipoint monitor measurements are also shown in the bottom of this figure. The monitor measurements on the edge of the chambers at $\phi = -11.25°$ are denoted by "o", while the measurements at $\phi = +11.25°$ are denoted by "+". The leftmost region of the plots shows the monitor data for superlayer #1, the middle region shows monitor data for superlayer #2, and the rightmost region shows monitor data for superlayer #3 (the points are shaded differently in these regions). The points are plotted in the sequence encountered when traversing the superlayer from left to right. The regions where the chambers are displaced is clearly visible. The top row of plots shows the data from the simulated stretched wire system, while the bottom row shows data derived via Eq. 11 from a simulated set of nested monitors. As mentioned earlier, both sets of measurements are identical.

The next example is generated by rotating a set of chambers at the $\theta = 90°$ edge of the hexant about the z-axis, and translating the middle layer's chamber at the $\theta = 30°$ edge of the hexant along the y-axis. The information from the projective monitors must thus be combined with the measurements from the multipoint monitors along z.

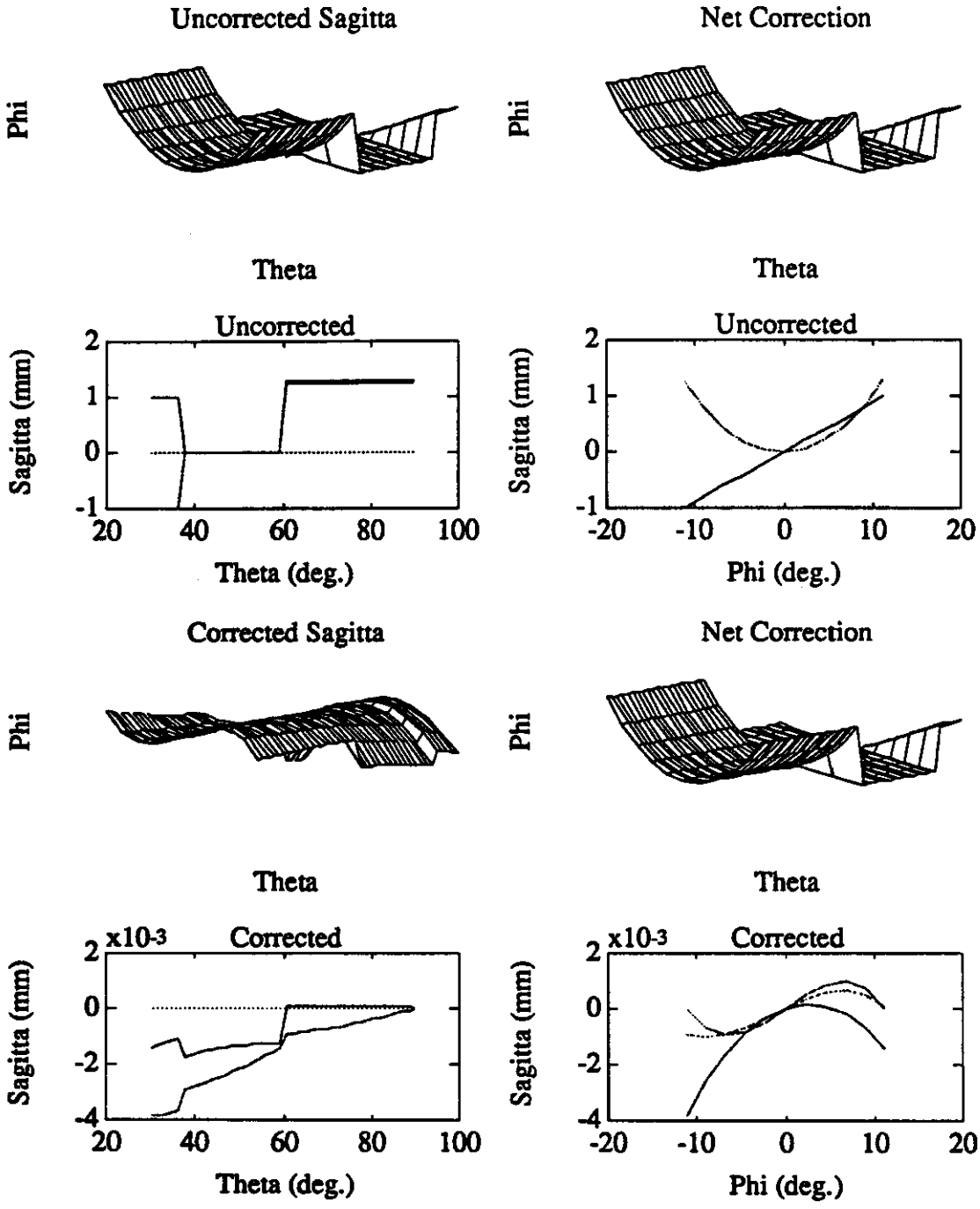

Figure 34: Sagitta error and correction for displacement of θ-edge chambers

The sagitta results are shown in Fig. 34. The sagitta error is again somewhat complicated, as the various chamber displacements are encountered across the θ range. The correction reduces the maximum error from roughly 2 mm to 4 μm. Interpolating the projective monitor measurements along z induces a θ dependance on the residual. Straightness monitor measurements are shown in Fig. 35.

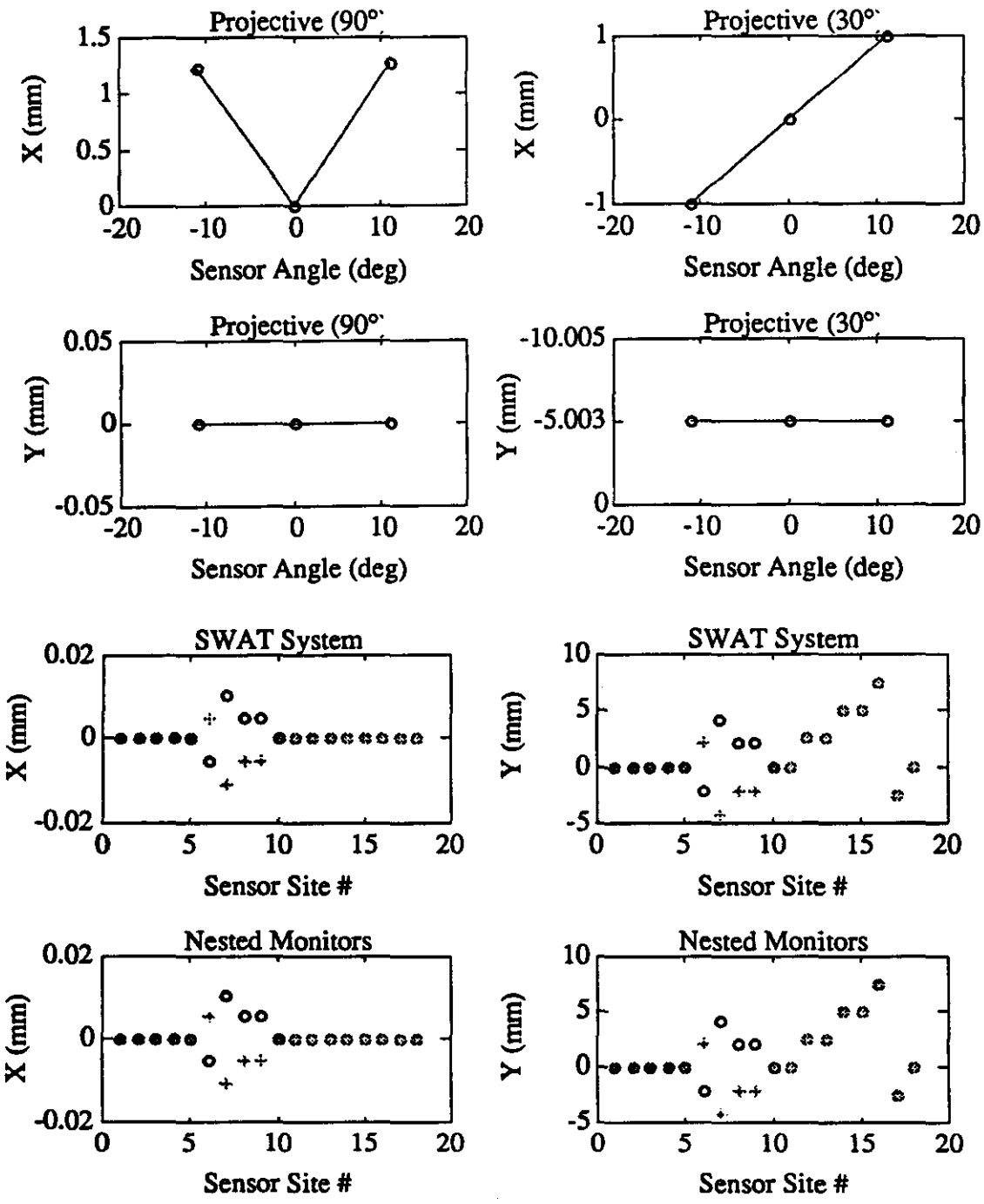

Figure 35: Straightness monitor measurements for displacement of θ-edge chambers

The next example takes this even further; all chambers and layers are translated and/or rotated about various axes (such as might be realistically expected). Sagitta results are given in Fig. 36, where we note a maximum error approaching 5 mm, distributed in a complicated fashion over θ and ϕ. The straightness monitor measurements (Fig. 37) are seen to reduce the sagitta residual to under 20 μm.

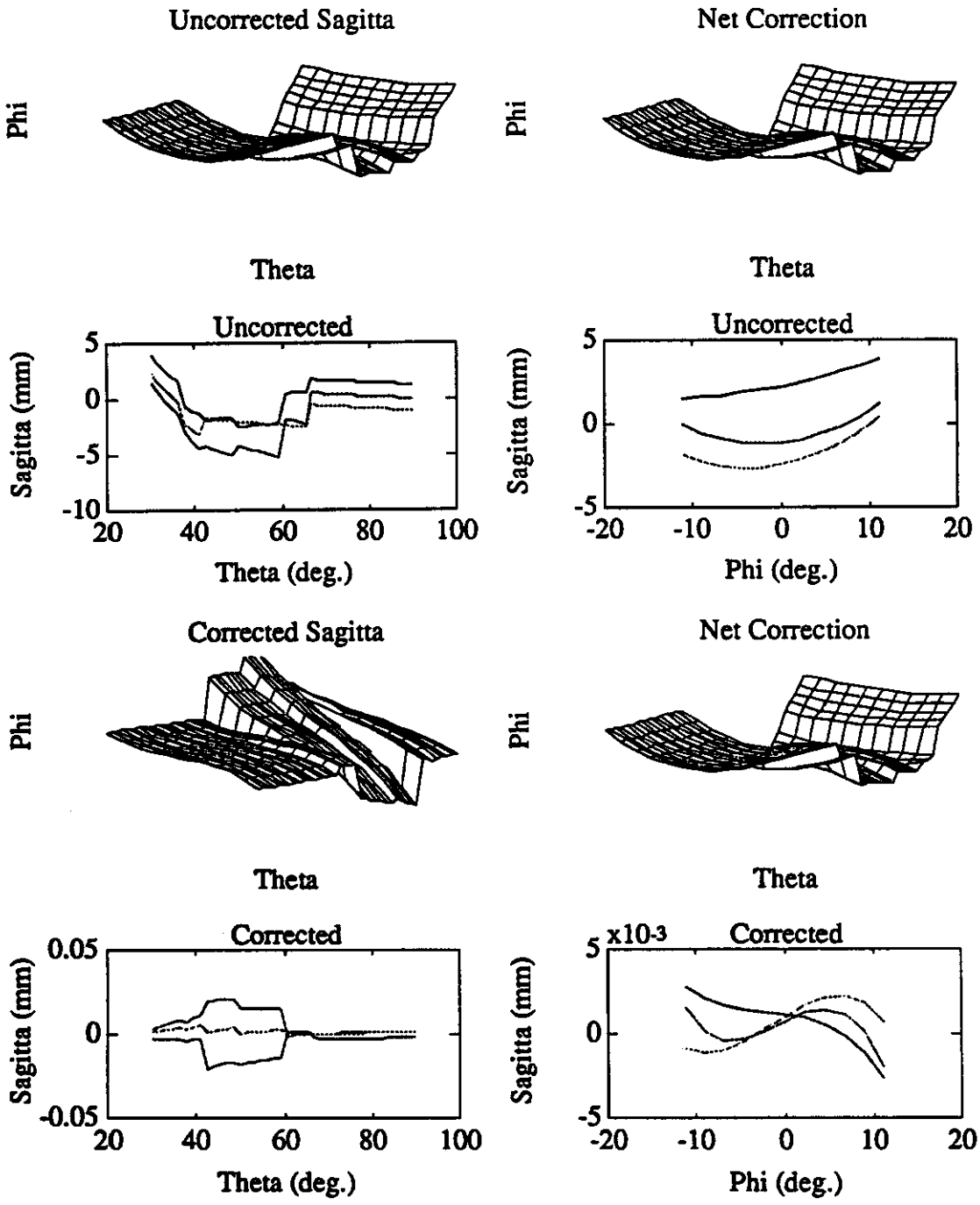

Figure 36: Sagitta error and correction for "random" deflections of chambers and layers

The final set of examples examine the effect on the alignment correction from global displacements of the hexant relative to the IP; i.e. where the interlayer monitors depart from a projective geometry, and no longer point along the straight-line muon path toward the interaction region.

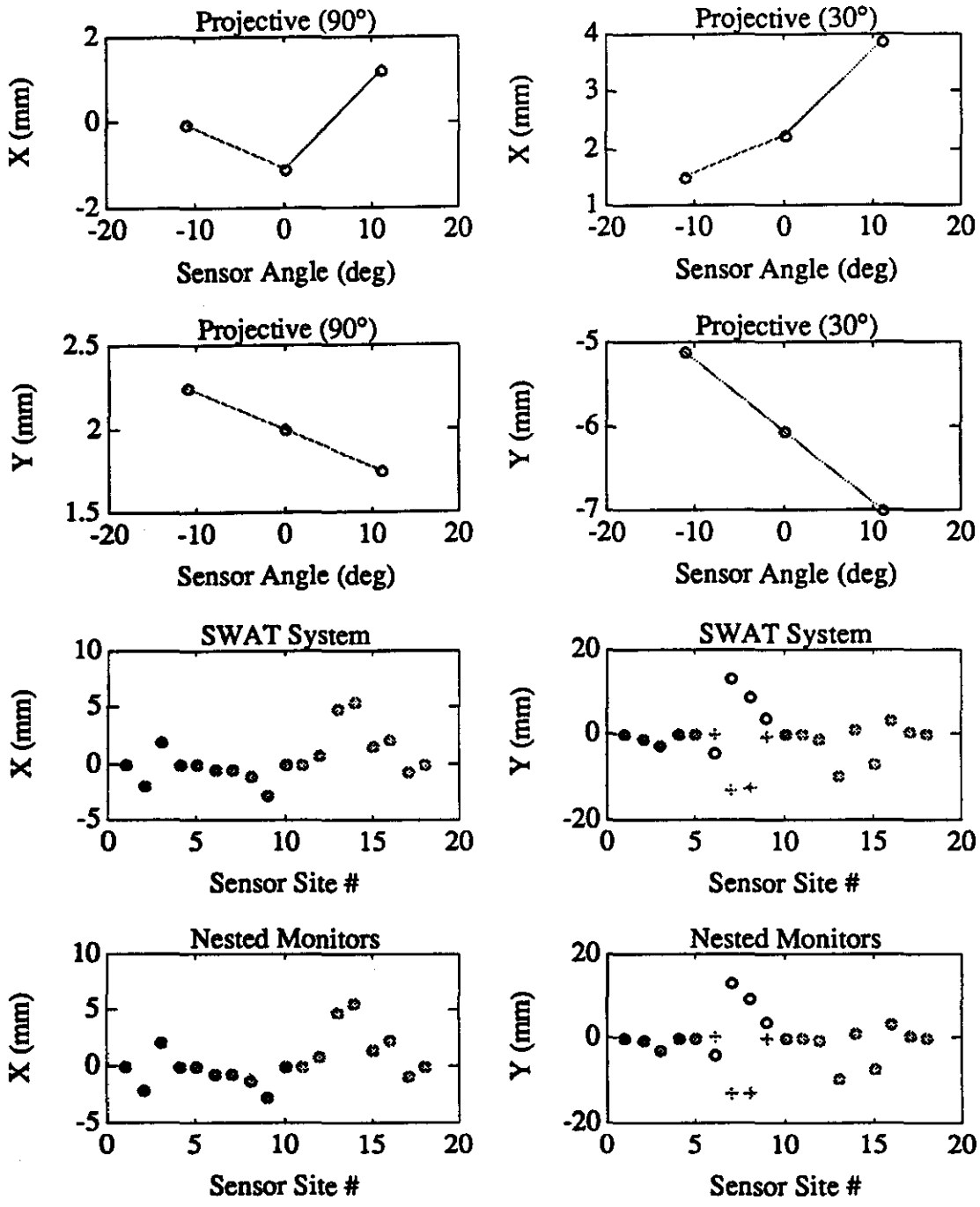

Figure 37: Straightness monitor measurements for "random" deflections of chambers and layers

This effect was examined in Ref. [1], although the analysis was not entirely based on a projective 3-dimensional system, as is simulated here. The effort of Ref. [1] looked at "torque" errors, where the straightness monitors yielded a null measurement, although the superlayers were displaced relative to one another (i.e. the layers were rotated by different amounts that kept the monitor axes straight, but changed their inclination).

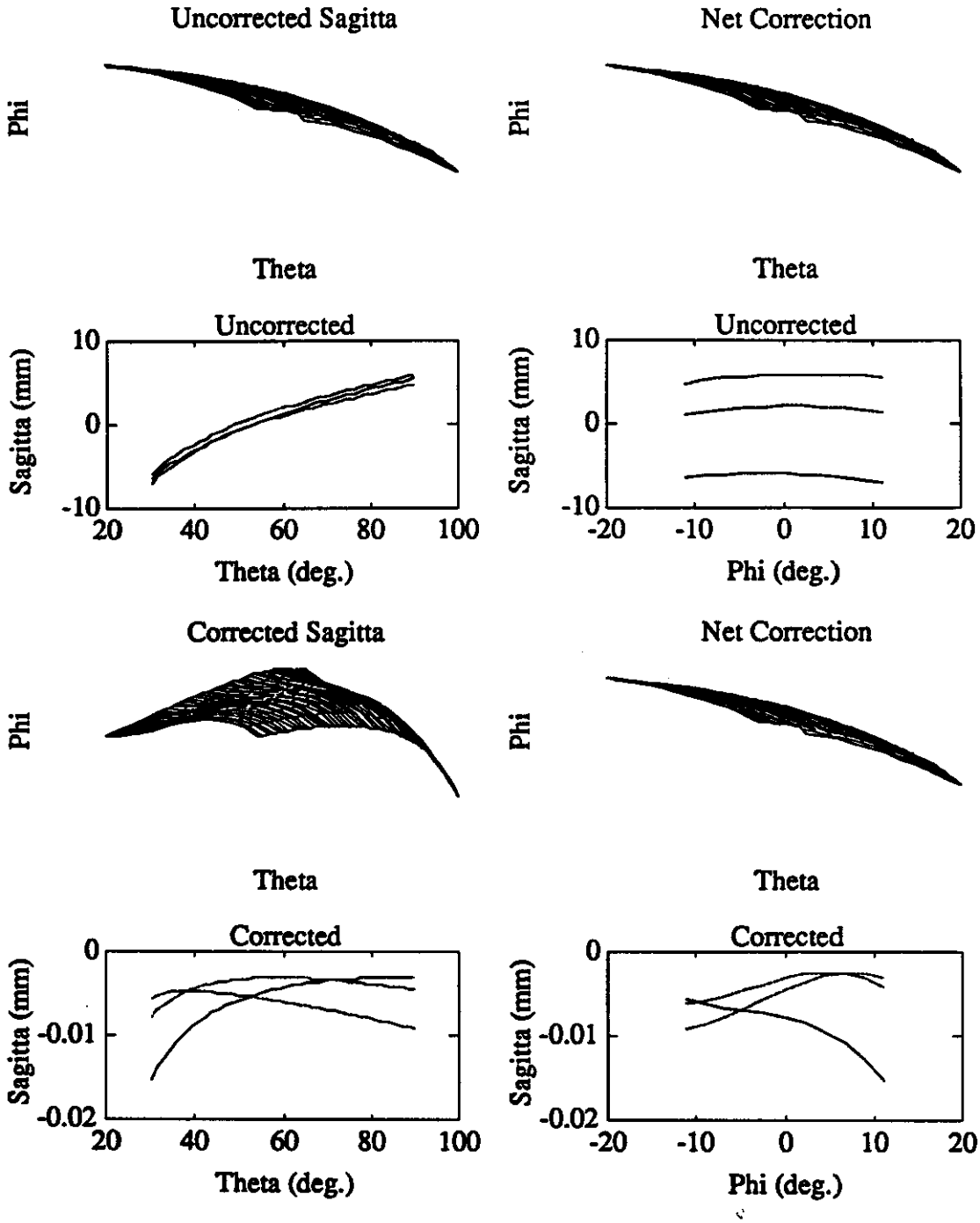

Figure 38: Sagitta results for skewed superlayers; projective geometry

Because of the projective geometry, obtaining null results for all six interlayer monitors simultaneously appears to be difficult without complicated scaling or deformation of the chamber planes, which would be difficult to realize in the current version of this simulation.

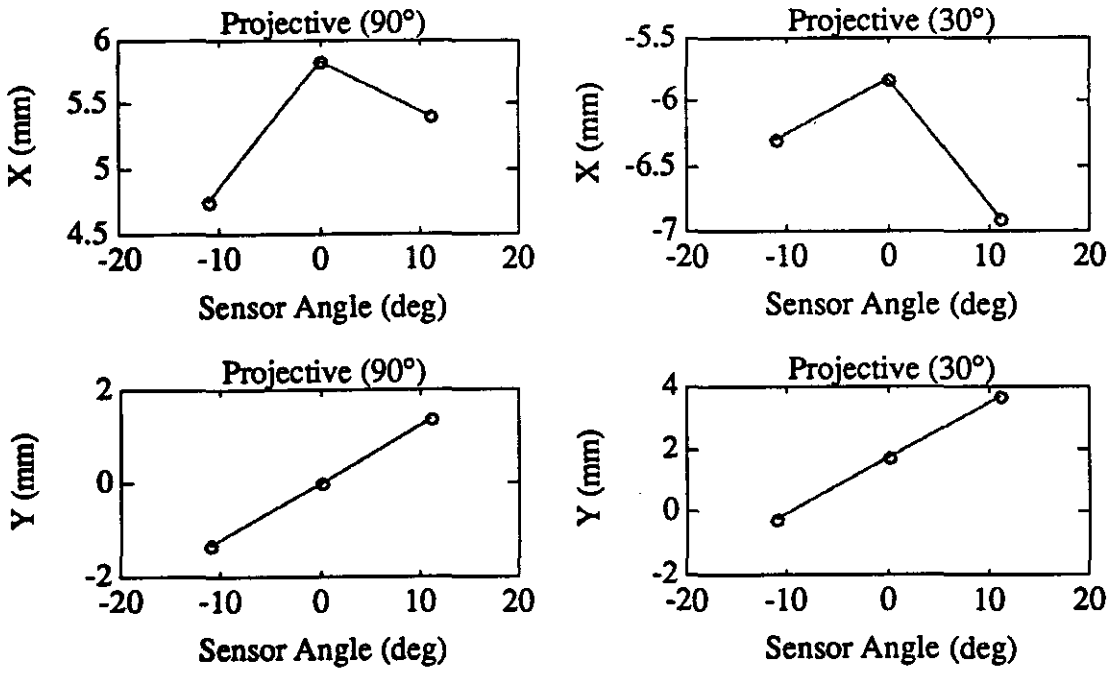

Figure 39: Interlayer straightness monitor measurements for skewed superlayers; projective geometry

Nonetheless, in order to look at various effects relating to the projective geometry, the three chamber layers were rotated in different axes (the outer layer by 1 mr about y, the middle layer by 5 mr about z, and the inner layer by 1 mr about z), thereby coupling all of the axes in the interpolations.

Sagitta results are shown for this example in Fig. 38; the uncorrected errors run up to a maximum near 10 mm, while the monitor corrections (Fig. 39) reduce these to under 15 μm (many of the effects illustrated in the previous examples are contributing to this residual). Figure 40 shows the residual for the same example, except the IP location is now offset along the x-axis by 5 cm. The maximum residuals are now considerably worse, ranging up to 40 μm (granted, a 5 cm error in this coordinate is perhaps excessive; the preliminary trigger requirements [1] are already on the order of 6 mm). Figure 41 shows the residual with the IP location now offset along y by 5 cm. A similar level of degradation is again noted, with the residuals now offset toward negative values, exceeding 50 μm. Figure 42 shows the residual with the IP location shifted along z by 5 cm. Less degradation is noted here, but the residual has definitely worsened, approaching a maximum around 30 μm. This coordinate will have an intrinsic smear of this order due to the anticipated size of the proton bunch envelope, thus the alignment monitoring and correction system must be robust to such shifts in the z origin of the muon tracks.

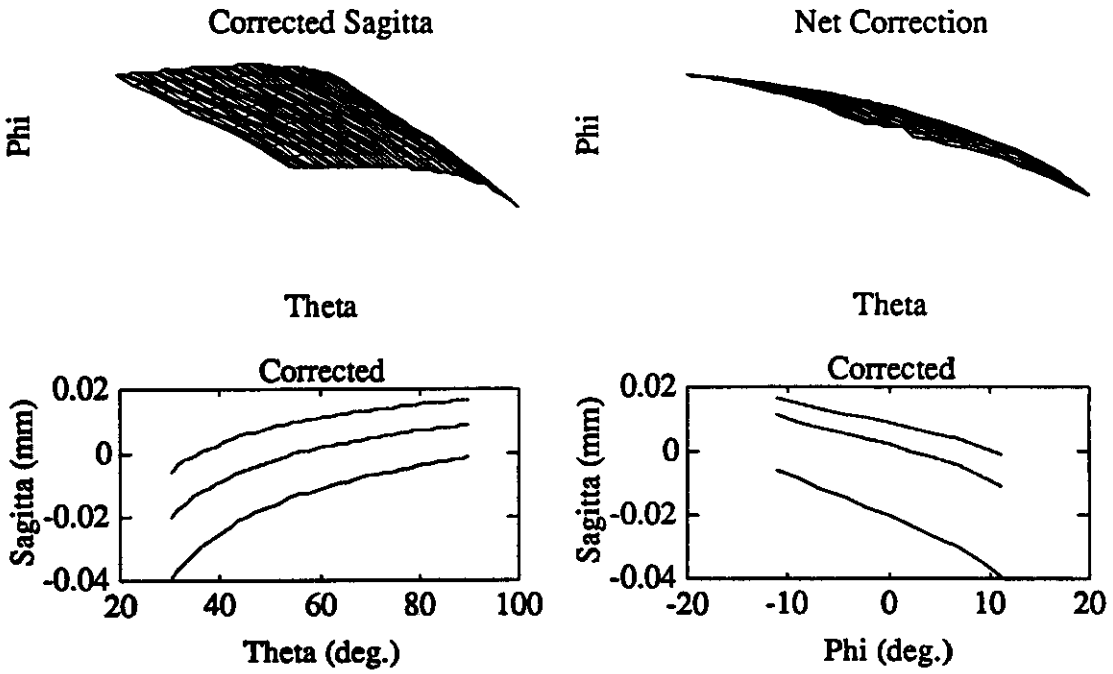

Figure 40: Sagitta results for skewed superlayers; IP offset by 5 cm in x

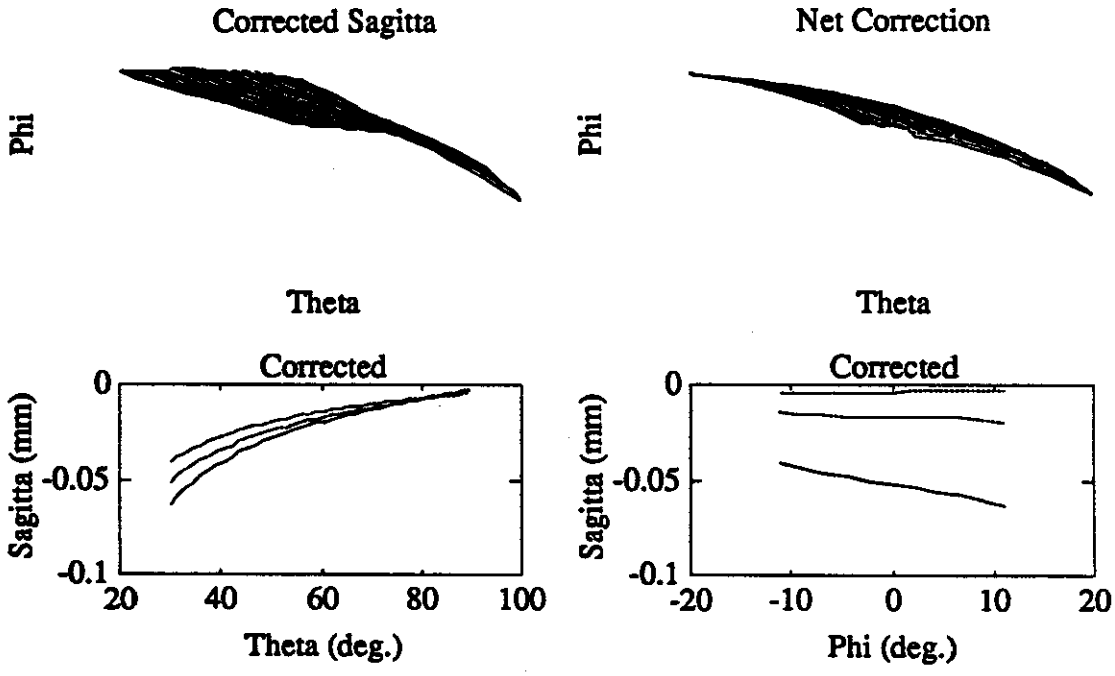

Figure 41: Sagitta results for skewed superlayers; IP offset by 5 cm in y

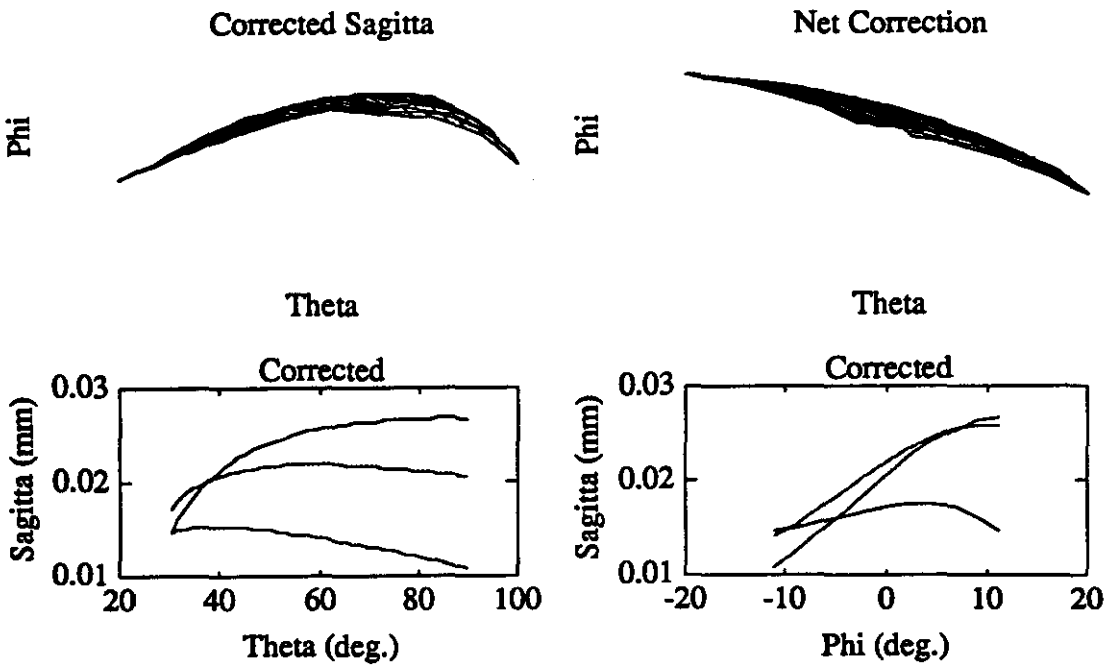

Figure 42: Sagitta results for skewed superlayers; IP offset by 5 cm in z

Granted, by examining a single set of chamber deflections (such as shown in Figs. 38-42), one can not make a blanket statement about sensitivities to non-projective alignment geometry; the sensitivities to displacements in each coordinate can vary according to the type of chamber misalignment. This example has generated an idea of the magnitude of this effect, and it seems surmountable (other projectivity requirements, such as in the trigger system[1] are potentially more stringent). The intrinsic bunch width, however, will limit the accuracy that can be attained with projective geometry along z, thus this may be a driver for keeping the chamber deflections under a couple of millimeters and maintaining rotations at the milliradian level.

3) Conclusions and Further Investigation

The simulation described in this report has only recently been developed, and all findings shown here are essentially initial impressions and observations. The postulated alignment monitors were seen to attenuate positioning errors projecting onto in the sagitta coordinate to the percent or permil levels (as experienced by a straight-line muon track originating at the IP). Nonetheless, the sensitivity of the correction function interpolated from a projective alignment system can be significant at the required level of accuracy

(i.e. 25 μm) for chamber deflections ranging near the currently anticipated 5 mm maximum[1,3]. These studies indicate that the required accuracy can be obtained if chamber translations are limited to the order of a mm and rotations restricted to the vicinity of a mr. Certain translations and rotations produce more effect than others, depending upon the type of chamber deformation that is encountered (thus it is difficult to set absolute limits on particular coordinates; i.e. the 1 mm and 1 mr constraints may be conservative for some chamber misalignments). The visual analysis of the correction residuals presented in Sec. 2 was also biased toward consideration of the peak alignment error across the hexant; in a true application, the RMS error may be of more quantitative relevance, thus this quote may again be somewhat restrictive. Regardless, this effort has indicated that the intrinsic residuals in these corrections hover at sufficient levels to warrant serious consideration.

Several corrections to the interpolation functions were proposed in Sec. 2 and tested in Sec. 3. While these were seen to improve the residuals for some hexant deformations, they added error for others (i.e. the net information remains limited in this system, and is only traded from one set of assumptions to another), thus their value is debatable in the current context.

A set of examples probed the sensitivity of this system to non-projectivity of the interlayer alignment axes. Little effect will be produced for pointing errors in the x and y axes below the cm level (as required for maintaining trigger efficiency[1]), and the IP smear along z expected from the finite bunch width will not introduce excessive error, provided that the chamber deflections are limited to the ranges sketched above.

The stretched-wire or nested monitor multipoint monitors were seen to be completely sufficient for correcting chamber positioning errors to a straight line between superlayer endpoints. The modelling of these components was somewhat ideal, however; noise and resolution effects were not considered, and chambers were considered to be rigid (i.e. a perfect glass bridge or solid endplate was assumed, producing no bending or nonuniform scaling). Errors were seen to be injected, however, from the z-interpolation between the projective monitor measurements at $\theta = 30°$ and 90°. These could be attenuated somewhat by correcting with the nonbending chamber measurements, provided that they are of sufficient accuracy (which is not currently baselined), or by backing out z errors from the alignment monitors (the scheme of Fig. 1 is under-instrumented for this, although it may prove more feasible for the all-projective system of Refs. [9,10]).

Future investigations should improve the modelling of the straightness monitors (i.e. include magnification and centroiding/transfer functions), and a noise/resolution

analysis should be performed for this system. Ultimately, an optimal estimator[11] should be constructed for candidate alignment schemes, with a model of the chamber deflections (positions to be estimated), plus the sensor models, geometry, and resolutions (expressed through a covariance matrix). In this fashion, redundant measurements can be appropriately blended (i.e. if the system of Fig. 1 were to add more projective lines between other sets of chambers, such as proposed in [9,10]), and the information from sagitta-orthogonal axes of the 2D-sensitive alignment detectors can be properly included. Such schemes could also serve to reduce ambiguities and extend the range of accurate sagitta correction.

Again, the chamber models assumed in this study were quite simple (i.e. planar), and the possible range of transformations were limited (i.e. purely linear). The expected types of chamber deformations and bending modes (as experienced by the sense wires and/or strips) should be included once they are determined for the preferred chamber technologies.

As mentioned earlier, the purpose of this analysis was to examine specific effects, and gain insight into the correction residuals for particular chamber displacements. The average sensitivity to all possible chamber displacements will be derived by iterating such an analysis with stochastically perturbed chamber packages, as in Refs. [9,10], with an accurate sensor model (this is prohibitive under the MATLAB interpreter[13] [in which this analysis has been coded], as its execution speed is too slow [particularly on a Macintosh-class machine] to gain sufficient statistics).

As a detailed alignment scheme is designed for the GEM endcaps, analysis packages similar to this (and the effort of [9,10]) should be assembled to likewise examine the validity of the sensor measurements and derived correction functions.

4) References

1) Paradiso, J., "Alignment Requirements for the GEM Muon Detector", GEM-TN-125, June, 1992.

2) G. Mitselmakher and V. Zhukov, "Alignment Requirements to Muon System", GEM-TN-92-120, June, 1992.

3) Paradiso, J., "Some Alignment Concepts for the GEM Muon Array", GEM-TN-92-124, June, 1992.

4) Toth, W. E., "Muon Detector Program; Prototype Octant Construction and Evaluation with Production Phase Recommendations", Draper Lab Report CSDL-R-1885, Oct. 1987.

5) Duinker, P., et. al., "Some Methods for Testing and Optimizing Proportional Wire Chambers", *Nuc. Inst. and Methods*, A273 (1988), pg. 814-819.

6) Sawicki, R., LLNL, "Muon Chamber Alignment Alternatives", Presentation at SSCL alignment meeting, June 12, 1992.

7) Wilson, I., "Alignment Studies for the CERN Linear Collider", CERN SL/92-41, August 1992.

8) Technical Design Report by the SDC Collaboration, SDC-92-201, Chapter 7, April 1992.

9) Mitselmakher, G. and Ostapchuk, A., "New Approach to Muon System Alignment", GEM TN-92-202, October 1992.

10) Mitselmakher, G. and Ostapchuk, A., "New Muon Chambers Alignment Scheme Based on Interpolation and Projective Geometry", presentation at the GEM/Muon Engineering Status Meeting at MIT, July 13, 1992.

11) Gelb, A., Applied Optimal Estimation, MIT Press, Cambridge, MA., 1974.

12) Fabre, M., "The Dimuon Mass Resolution of the L3 Experiment at LEP and its Dependance on the Muon Spectrometer Alignment", Thesis, ETH Zurich, Institute of High Energy Physics, Diss. ETH Nr. 9696, 1992.

13) MATLAB, version 3.5, The Math Works, Inc., Cochituate Place, 24 Prime Parkway, Natick, MA. 01760.

14) Zhukov, V., "GEM Muon Alignment Requirements Summary", June, 1992.

15) Newman, W.M. and Sproull, R.F., Principles of Interactive Computer Graphics - 2'nd edition, McGraw Hill, New York, 1979.